The Design of Zinc Metal Organic Frameworks for Biomedical Drug Delivery

Alec Bigness

April 25th, 2019

Florida Southern College, 111 Lake Hollingsworth Dr, Lakeland Fl 33801

Abstract

A vast library of zinc metal-organic frameworks (MOFs) have been prepared and evaluated for their use in pharmaceutical drug delivery. Their properties and structures have been modulated through the variation of reaction conditions like solvent, starting material ratios, and method of reaction. A novel metal-organic framework, AB MOF1, was successfully prepared and characterized by x-ray diffraction analysis. AB MOF1 was evaluated for its use in drug delivery by using the model pharmaceutical drug ibuprofen for uptake studies, and AB MOF1's stability in common biological and medicinal solvents was evaluated through Powder X-ray Diffraction (PXRD). The evaporation of ibuprofen at 157 ^{o}C during Thermal Gravimetric Analysis (TGA) of AB MOF1 impregnated with ibuprofen along with the change in morphology of AB MOF1 using PXRD give a likely indication ibuprofen was absorbed into AB MOF1. The uptake of ibuprofen reached capacity after fourteen hours of stirring in an ibuprofen solution, and the uptake is comparable to previously published results. Computational DFT studies corroborate the fact that the interaction between ibuprofen and AB MOF1 is favorable. The energy of interaction, which is defined as [(energy of AB MOF1 with ibuprofen) - (energy of ibuprofen alone + energy of AB MOF1 alone)|], of the zinc paddlewheel motif and ibuprofen was calculated to be 1.030 kcal/mol, which substantiates that the interaction between ibuprofen and AB MOF1 is favorable. This work shows the promise of AB MOF1 as a novel drug delivery vessel, and further prove the efficacy of using metal-organic frameworks to uptake and release pharmaceutical drugs in biomedical applications.

Introduction

Although cancer treatments have reduced the cancer mortality rate by 13% from 2004 to 2013[1] there are still many adverse side effects that result from chemotherapy and radiation treatment[2]. An anti-cancer drug's primary goal is to stop unregulated cell proliferation, but selecting between healthy or cancerous cells is still a major challenge for the pharmaceutical industry. A textbook example of a common chemotherapy drug, Taxol, stops cell proliferation by binding to microtubules which play a major role in cell replication[2]. Since spindle microtubules allow for separation of chromosomes in mitosis and meiosis, damage to these would pose a considerable threat to healthy tissue as well. Creating a more selective method of administration can improve the pharmacokinetics of the host drug, which can be accomplished through targeted drug delivery.

This issue of problematic pharmacokinetics does not just affect anti-cancer drugs however; this phenomenon affects every major blockbuster drug treatment for conditions like diabetes mellitus[3], hypertension[4], parkinson's disease[5], and hyperlipidemia[6]. There are many varying causes to poor pharmacokinetics, yet some of the most common are low oral absorption through the gastrointestinal tract[7], rapid excretion through the body[8], or difficulty crossing the blood-brain-barrier (BBB)[6]. Due to the chemical properties of each pharmaceutical drug, each issue is specific for the case, but two of the main limiting issues in pharmaceutical development are sustained drug release[9] and optimal oral bioavailability[10] – it is painful for physicians, patients, and pharmacists when a high dosage of drug must be prescribed and taken often. Since oral delivery is considered the easiest and thus the gold standard of drug administration[11], researchers and pharmaceutical companies forever search for the unicorn compound that is

absorbed orally with a high bioavailability, possesses an optimally long half-life, carries few side-effects, and of course offers its intended therapeutic effect.

An interesting solution to this issue is targeted drug delivery, where a host compound is used to encapsulate guest pharmaceutical drugs. By distributing a drug to specific intracellular or extracellular target, drug delivery vessels protect healthy cells and improve drug bioavailability by binding to either receptors or other recognizable sites. Some of the first introduced drug delivery systems were nanoparticles[12]. The shape, size, and modification of nanoparticles can be changed by simple modifications in experimental synthesis. For instance, the ability to encapsulate with folic acid, target cancer cells, and then promote cell death through apoptosis was shown using iron oxide (Fe_3O_4) nanoparticles with added carbon dots[13]. In addition, inherent properties like the nanoparticles' size increases their ability to effectively penetrate tissues at the molecular level, pass through biological barriers, and easily bind modifications for cell recognition, showing the multifaceted benefits of using nanoparticles and other nano-sized discrete structures as vessels for drug delivery[14]. However, with inorganic iron oxide nanoparticles, there are many issues like nanoparticle agglomeration, poor drug loading, and the possibility of oxidation from Fe_3O_4 to Fe_2O_3. Liposome systems were the first investigate mode of drug delivery, yet they too experience difficulties like liver sequestration, vesicle destabilization, and enhance permeability and retention (EPR) effect[15]. Even though these systems have been investigated for over 50 years, they still have only seen incremental and scattered use in real world applications[16].

Metal-Organic Materials as an Alternative

Most of the researched mechanisms of drug delivery can be divided into two divisions – inorganic nanoparticles and organic liposomes and polymers[16]. However, less attention has been given to metal-organic frameworks (MOFs), whose high porosity and surface area make them excellent candidates as drug delivery vessels. *Horcajada et al* presented a validation of metal-organic frameworks for controlled drug release through studying their interaction with the model drug ibuprofen[17]. The **MIL-53 MOF** (MIL standing for Material Institute Lavoisier, 53 for the 53rd MOF created) was used for its inherent flexibility between a third oxidation state Fe or Cr metal and terephthalate ligand[17]. Rigorous characterization confirmed the adsorption and release of ibuprofen; Powder X-ray Diffraction (PXRD) showed **MIL-53** before and after release of ibuprofen, Nuclear Magnetic Resonance's (NMR) high anisotropy showed the interaction between ibuprofen's carbonyl bond and the hydroxide on the MOF's metal center, and Infrared Absorption (IR) Spectroscopy coupled with Density Funcitonal Theory (DFT) also confirmed that the ibuprofen molecule had a hydrogen bonding interaction with the hydroxide on the metal center[18]. After validating ibuprofen controlled delivery via MOFs, *Horcajada et al* investgated MOFs for anticancer and anti-HIV pharmaceutical drugs[19]. The highest adsorption of drug was seen with the **MIL-100** and **MIL-101** MOFs reaching absorption values up to 90%. These promising results show the support that periodic MOFs are a burgeoning field that has a high upside in sequestering and delivering pharmaceutical drug molecules.

Structure Property Relationships: Design with Shape in Mind

Pharmaceutical drugs are extremely insular and difficult to group together – what may work for one drug may not be prudent for another. That is why whatever material that is proposed for drug encapsulation must be flexible to adapt and change to each drug to improve drug absorption and

release. With a seemingly infinite amount of options from metal type to organic ligand linker that influences their three-dimensional assembly, new metal-organic polyhedra (MOPs) structures are being published at an accelerated rate[20], showcasing their ability to quickly modulate chemical, electronic, and supramolecular properties. Before continuing any further, the nomenclature of these various acronyms should be addressed due to their confusing nature. Metal-organic materials encapsulates all metal-organic hybrids and is a larger umbrella term. Metal-organic frameworks (MOFs) are a type of MOM that exhibits a repetitive, periodic structure that resembles a porous three-dimensional cage, while metal-organic polyhedral (MOPs) are discrete, singular structures with a defined three-dimensional polyhedral morphology.

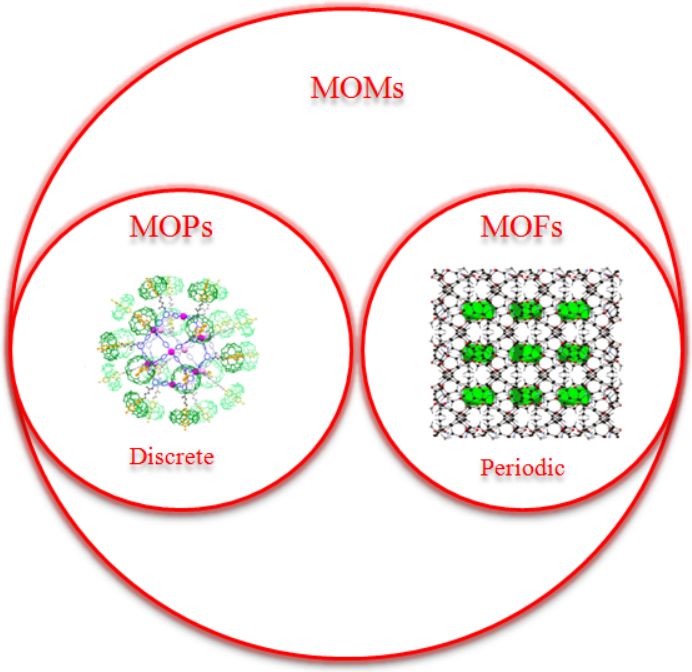

Figure 1: Venn Diagram that illustrates the terms that are often used in the research of hybrid metal-organics. MOM is an umbrella term that describes any metal-organic compound, while MOPs and MOFs differ on their arrangements; MOFs are repetitive and periodic, while MOPs are discrete and one functional unit is not covalently linked to the next.

Metal-Organic Polyhedra (MOPs)

Metal-organic polyhedra, as the name entails, are defined as a metal to ligand bond that assembles and proliferates into a polyhedral structure[20]. Due to the variation of polyhedra, it is expected that MOPs have a vast array of classifications, ranging from Platonic MOPs (highly symmetric tetrahedrons, hexahedrons, and icosahedrons), semi-irregular Archimedian MOPs (i.e. cuboctahedron, snub dodecahedron, and truncated cube), faceted MOPs , and stellated (*stella octangula*[21]) MOPs[20]. Their ease of production and high symmetry can be further applied as supramolecular building blocks (SBBs) for MOFs[22], where the nanoscale structure of a discrete MOP is polymerized into a three-dimensional, periodic MOF structure. SBBs can be visualized as smaller repetitive structures of high symmetry creating a larger three dimensional structure (as seen in **Figure 2** where copper MOPs are linked together into a larger framework)[22]. Linking MOPs as SBBs for MOFs has proven to be effective in the drug delivery of 5-flourouracil[23], a topically applied anti-cancer suicide inhibitor class drug.

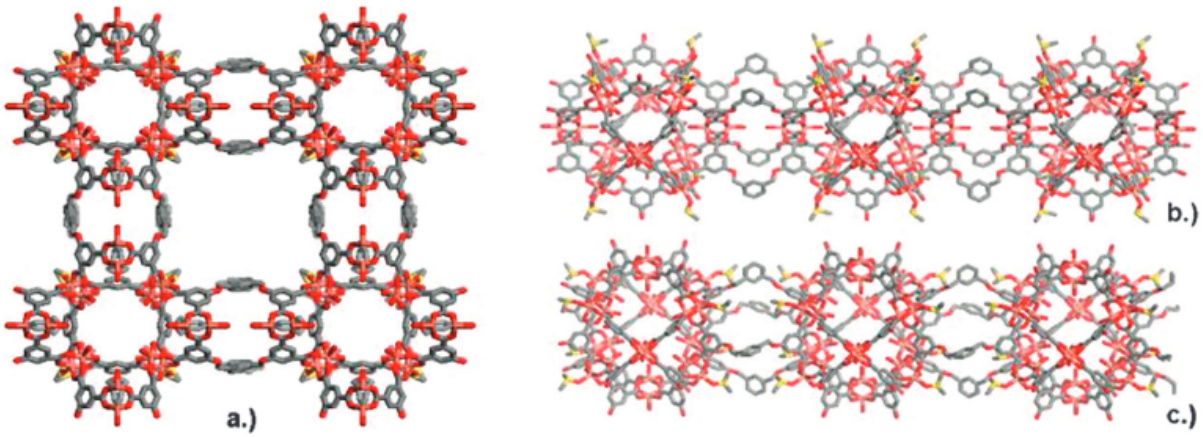

Figure 2. Illustration of MOPs acting as SBBs in a larger metal-organic framework: (a) ab plane of copper nanoballs by quadruple linking (b) cross-linking across a and b axis in syn-formation (c) cross-linking shown in anti-formation[22]. Reprinted (adapted) with permission from: Perry IV,

J. J., Kravtsov, V. C., McManus, G. J., & Zaworotko, M. J.. *Journal of the American Chemical Society*, **2007**, *129*(33), 10076-10077. Copyright 2007 American Chemical Society.

Synthesis Strategies

Facile synthesis like solvothermal methods and room temperature reactions can create high symmetry metal-organic polyhedra colloquially referred to as "shake-and-bake", where reagents are mixed together and set in an oven. Due to the ease of experimentally creating MOP structures and their elegant aesthetic, MOPs show promise as simple molecular architectures that can be used as cage-like nanomaterials or SBBs for MOFs[24]. Creating these MOP structures is exactly similar to how one would build a polyhedron, either you assemble the faces together, or one can focus on connecting vertices to generate polyhedron structures. These are referred to face-directed synthesis and edge-directed synthesis respectively, where rational design strategies based on the three dimensional shape of the metal and organic linker detail how they will puzzle together in a discrete form. Both of these methods usually depend on the three-dimensional structure of the materials, and do not exclusively depend on synthesis methods. During face-directed synthesis, organic linkers span the two dimensional faces of the structure, and the metal is present at the vertices[25].

For edge-directed systems, linear components are directed towards the corners of a structure[26]. Opposite to face directed synthesis, edge directed synthesis focuses on the edges of a polyhedron. Thus, the organic linkers will not be present on a face, but on an edge linking metals on the vertices. For example, an edge-directed copper paddlewheel MOP was constructed with Cu(II) and C_2 symmetry pincer like ditopic ligands that created a C_4 symmetry tetragonal cage (**Figure 4**). The benzene and alkyne moieties of the ligand increase the rigidity of the structure at

the vertices and allow for stable edge-directed synthesis[27]. Miniscule changes on the regiochemistry of a metal coordination center can quickly change the three dimensional shape of the metal-organic material; for instance, changing a *cis*-$InN_2(CO_2)_4$ Kagome two dimensional lattice to a *trans* orientation results in a discrete *trans*-$InN_2(CO_2)_4$ octahedron[28]. Understandably, there are many factors a synthetic chemist can modulate in order to generate a completely novel molecular structure.

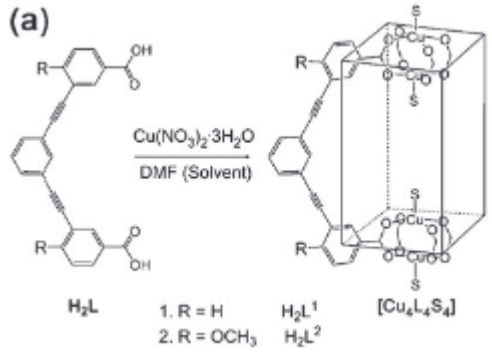

Figure 4. A reaction scheme for the self-assembly of augmented tetragonal MOPs[27]. The organic linkers span the edges of the rectangular prism. Reprinted with permission from the Royal Chemistry Society Publishing and *RSC Chemical Communications*.

Modification Strategies

Not only are there many synthetic strategies to change supramolecular geometries of MOFs and MOPs, but there are many ways that existing compounds can be functionalized further. Creating complex supramolecular assemblies with specific applications has proven to be difficult. That is why over the years researchers have started employing post-assembly modification (PAM) to both MOFs and MOPs. This technique allows for tunable aspects of the metal organic hybrid's ligand linkers to be modified by maintaining the base polyhedral structure of the compound. Previous work has shown that covalent and non-covalent modifications of MOPs can be done as a PAM, *Samanta et al* was the first to show the use of both on one MOP

that has many applications as a biologically relevant nanocage[29]. 2-(Cyclooct-2-yn-1-yloxy)-N-[3,5-di(pyri-din-4-yl)phenyl] acetamide was used to synthesize the organic linker for the MOPs, later referred to as **Compound 1** (**Figure 5**). These structures then underwent a PAM with a strain promoted alkyne azide click reaction and a host-guest exchange non-covalent interaction. The strain promoted alkyne azide click reaction was used with **MOP 3** and a number of biologically relevant compounds like Biotin, PEG350, and Sulfonate that showcases its applicability as a nanodrug carrier through PAM. A "click" chemistry MOP was created with copper-isophthalate nanoballs that added azide terminated polyethylene glycol that turned the MOPs into colloids and assisted in delivery of 5-flourouracil[30].

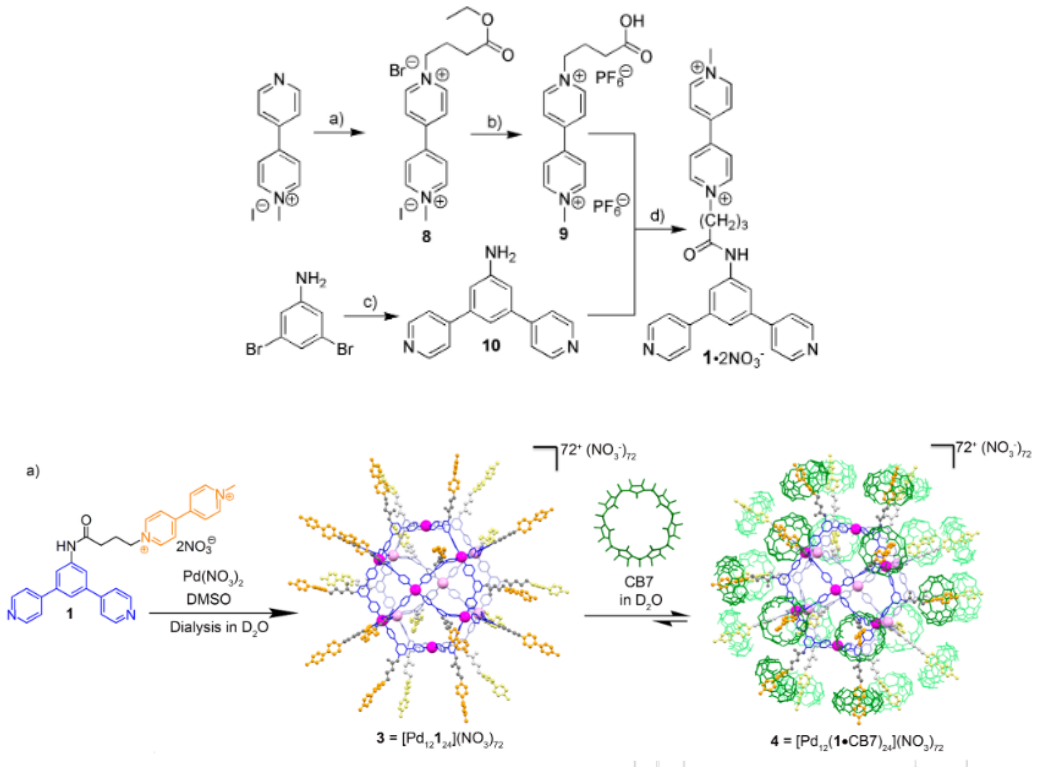

Figure 5: (top) synthesis schema of compound 1 ligand from *Samanta et al*[29]. Synthesis schema of $[Pd_{12}\mathbf{1}_{12}](NO_3)_{72}$] which is then added CB7 groups via post-assembly modification to make

$[Pd_{12}(\mathbf{1}\bullet CB7)_{24}](NO_3)_{72}$ shown on the far right. Reprinted with permission from John Wiley and Sons and *Helvetica Chimica Acta*.

This group also investigated large palladium MOPs that have 24 methyl viologen units for covalent outside attachment of doxorubicin[31] (**Figure 5).** Proton NMR confirmed that the napthalene protons underwent a chemical shift that indicates binding. *In vitro* cytotoxicity was monitored through confocal fluorescent microscopy of incubated samples of **MOPS 2** and **7**[31]. Similarly, others have integrated polymers and discrete MOP structures to tailor their growth[32]. These metal organic polyhedral were confirmed via single crystal x-ray to have a general formula of $[Cu_{24}(m\text{-bdc})_{24}(S)_{24}]$. A Polyethylene glycol polymer coordinated to a discrete copper MOP was used to control the structure's overall growth and orientation. These methods altogether detail the expansive amount of morphologies and methods that can be utilized in creating novel MOPs and shows there is still a wealth of information to be obtained in this area. However, when using these structures for biological applications, what aspects should experimentalists look out for?

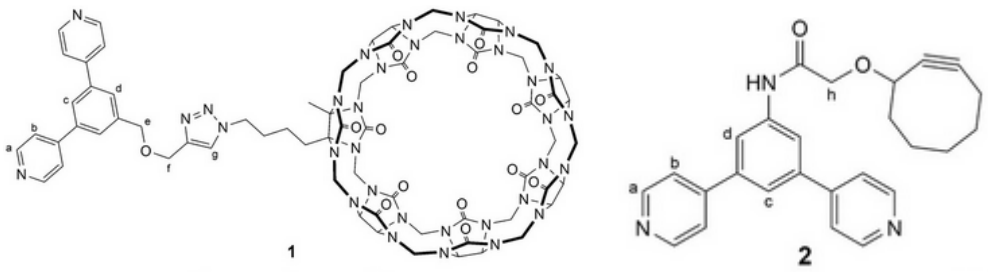

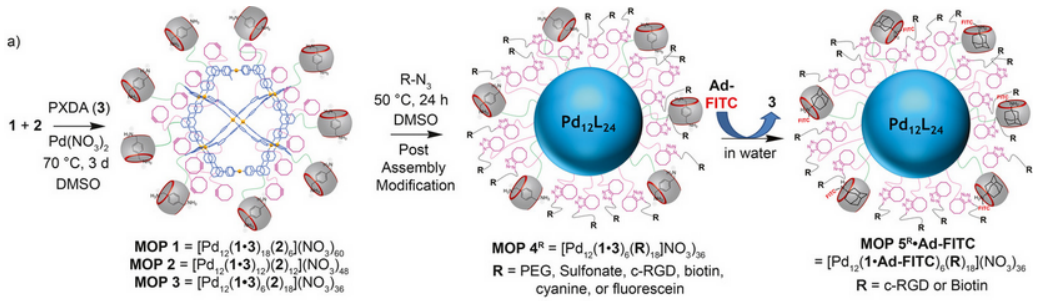

Figure 5. Schema of PAM azide click reaction for $Pd_{12}L_{24}$ MOPs from Compounds 1 and 2. Palladium nitrate when in the present of Compound 1 and Compound 2 creates a discrete polyhedron with large bispyridine ligands on the exterior. These ligands were then modified with various R groups like sulfonate, biotin, or fluoroscein[31]. Reprinted (adapted) with permission from: Samanta, S. K., Moncelet, D., Briken, V., & Isaacs, L. *J. Am. Chem. Soc.*, **2016**, *138*(43), 14488-14496. Copyright 2016 American Chemical Society.

Translation to Biology

When considering biological applications of MOFs, it is apparent that using harmful metals is immediately disregarded. Most materials will have to deal with smaller, relatively safer transition metals like calcium, magnesium, zinc, and iron. Thus, when choosing potential MOMs to synthesize for drug delivery it is important to design structures with lower toxicity and higher stability. Unstable materials could result in excess metal ions or harmful organic compounds present in high blood concentration. However, this has not been a concern for the metal-organic materials community since there are few results that report toxicity issues of MOMs[33]. It is preferable to use organic linkers that are familiar to the body, yet endogenous linkers that are commonly used for MOFs are non-toxic as well. Terephthalate, trimesic, 2,6 napthalenedicarboxylic acid, and 1-methylimidazole all have and LD_{50} above 1 g/kg (1.13, 5.5, and 8.4 g/kg respectively; where LD_{50} is defined as the lethal dose to kill 50% of mice)[33].

Structures containing endogenous organic ligands like **MIL-88**, a three-dimensional iron(III) fumarate[34], or iron(III) carboxylate[35] showcase the ease of combining biologically safe molecules into three-dimensional porous structures.

Additionally, most polymeric MOFs have microporous openings that are too small for efficient uptake of larger pharamaceuticals. Materials must contain a larger mesoporous structure that has been shown to be more efficient in drug loading. The **MIL-53 MOF** was one of the first metal-organic materials to boast this quality that owed its size to its flexibility and size of organic ligands[17]. Using MOPs as building blocks for larger porous materials has proven successful in encapsulating 5-Fluorouracil, an anti-cancer drug plagued by low aqueous solubility and difficulty passing the skin barrier[30]. Many metal-organic materials aim towards encapsulating and delivering 5-Fluorouracil[30,36]. Successful endocytosis of metal-organic polyhedra was shown by imid-azolate nanospheres that could encapsulate fluoroscein, camptothecin, and iron nanoparticles[37]. Others have looked into covalent attachment of antibiotics, where a doxorubicin prodrug was attached on the outside of a MOP[31].

Copper Structures

Although copper is not a biologically safe metal since its lethal dose is comparatively low, it is a versatile metal that adopts an octahedral geometry that is favorable for forming metal-organic polyhedra. Previous studies have shown copper and a 5-hydroxyisophthalic acid ligand to form discrete nanocages through room temperature self assembly[38]. *Zawarokto et al* reports that a *small rhombihexahedron* geometry formed between copper and 5-hydroxyisophthalic acid with a volume of 10 nm^3, which are all ideal dimensions for a possible drug delivery vessel[38]. The room-temperature layering synthesis aims to create “faceted” polyhedra, meaning the MOMs are

shapes constructed of smaller polygons by linking their vertices. These "faceted" polyhedra specifically refer to those structures that have both concave and convex faces, and the created three possible faceted polyhedra in ranging size: *cubohemioctahedron< small rhombihexahedron< small rhombidodecahedron*. Studies into the solution stability of the copper nanoballs highlight their impregnable structure – there was no significant degradation found for temperatures up to 60 ºC and ambient pressure to 3.5 kbar[39]. A significant loss of intensity in the charge transfer band is seen above a mole fraction of 0.7 water:methanol solution, but below 0.7 the nanoballs retain their stability. From the pH of 5-10, the nanoballs were stable, but beyond these pHs the ligand was protonated and hydroxide ions disrupted the structure, respectively.

Zinc Structures

Zinc hybrid materials and their promise as biologically safe MOMs since they address many of the aforementioned issues of metal toxicity. Its lower toxicity as a metal shows promise – groups have utilized inc with biologically prevalent ligands like the base unit adenine in creating biological metal-organic frameworks (bio-MOFs) that retain crystallinity in biological buffers for extended periods of time[40]. Additionally, zinc is a relatively cheap metal that shows promise for industrial and medical applications. Other studies of adenine base ligands show that these zinc MOFs posses pH tunable release[41]. These lower levels of toxicity and high capacity for drug loading make nanoscale MOFs a promising alternative to previous drug vessels.

Few papers have published results of a zinc MOF that incorporates the metal with a 5-hydroxyisophthalic acid ligand. A tetrahedral ZnO_4 MOF linked with benzenedicarboxylate ligands has been synthesized previously[42], but it has proven elusive to create a discrete zinc structure. An endogenous imidazole linker generated eight separate three-dimensional gmelinite

(**GME**) geometry boasting pore diamters up to 16 angstoms[43]. The synthesis of a polymeric MOF used zinc and manganese with a 5-hydroxyisophthalic ligand in the past, but this was done with reactions in high temperature and pressure systems[44]. Ultimately this can lead to thermodynamically favored products with a higher order of crystallinity, but this would introduce size problems associated with compounds outside of the nanoscale range. Other methods have produced a 2D net using zinc and 5-hydroxyisophthalates, but this again violates the nanoscale size specifications for biologically available drug vessels[45].

The zinc metal-organic materials discussed in this section thus far have been polymeric; few discrete metal-organic polyhedra and other discrete zinc structures have been reported. Since these structures are not discrete, but rather periodic or repeated, they large size prohibits their ability to work effectively in biological systems. Distribution around the circulatory system and absorption through oral administration is thus very difficult with large crystalline structures. This suggests that there is a need to further investigate zinc metal materials as possible drug delivery vessels. Although Horcajada et al reported the investigation of Fe and Cr (III) MOFs as drug delivery vessels, few researchers have published work on zinc MOFs or MOPs to uptake and deliver drugs. The lack of literature available could possibly indicate an area that is outside of the wealth of scientific knowledge. The safety of zinc as a biological metal combined with the structure of previously synthesized structures could prove to be an applicable material and requires interest.

Computational Studies

Computational work has been used for years to supplement the work of experimentalists and elucidate mechanisms, structures, or processes that cannot be observed in the lab. The same

goes for metal-organic materials, but since the field does exhibit massive often periodic structures, theoretical researchers have utilized different methods to obtain meaningful data from metal-organic systems. Since most *ab initio* calculations are done with organic molecules in mind, most transition metals have received less attention and thus it is more difficult to choose the right computational parameters. Previously, *ab initi*o calculations were done on organic molecules ranking the standard deviation of optimized calculated geometries from experimental values, allowing computational researchers to compare which parameters were the most effective. This was not yet done for transition metal complexes, so *Bühl et al* calculated optimized geometries on a number of organmetallic transition metal compounds, trying a multitude of density functionals and basis sets to statistically determine which was the best in calculating the correct geometries[46]. Of the GGA functionals, which are the most basic and least rigorous, the BP86 density functional was the most effective in consistently predicting the geometry of the transition metal complexes. Surprisingly, B3LYP, which is common density functional many use in density functional theory (DFT) calculations, was one of the least accurate with values that far exceeded correct bond length values. The most accurate was the meta-GGA TPSS functional, which is computationally demanding, but garners the most accurate results.

Since DFT scales well and is known for its ability to predict equilibrium geometries, it is the theory of choice for the large metal-organic materials. Not only the large transition metals present a problem, but simulating periodic structures requires a separate theory like a plane-wave basis set[47]. This is a circular problem yet because a plane-wave basis set requires psuedopotentials to be efficient, which is not friendly with first row transition metals. Although DFT is an accurate and rigorous derivation of *ab initio* methods, it quickly becomes inefficient in

simulating even a unit cell of a MOF. This scale of calculation is possible for DFT methods, but it is often computationally exhaustive and expensive. Theorists have thus reduced MOMs to their discrete repeating units and run calculations from that repeated structure. For example, *Teo et al* reduced hetero-bimetallic paddlewheel complexes to their functional paddlewheel to estimate the interaction between hydrogen and the metal complexes for applications into hydrogen storage[47]. Due to this, MOFs energies and optimum geometries were calculated with a metal coordination cluster set to periodic conditions[47]. This minimizes crucial computational power and allows for more rigorous basis set and theory to be utilized. A heterobimetallic MOP was synthesized with Ni, Zn, or Cu with a square planar Pd in a paddlewheel node was calculated in the same fashion[47] . Ultimately for a higher order molecular orbital study, it is only possible to reduce the structure down to its lowest common denominator[48]. More efficient methodologies and computational power in the future will allow for more holistic, accurate studies on the interaction of large scale metal-organic materials and pharmaceuticals.

Although DFT is proficient in estimating electronic density and energies of chemical structures, it has been a long held criticism that it is not effective in determine intermolecular forces. In the past, this may have been correct, but several papers have now investigated how accurate certain density functionals are at predicting hydrogen bond lengths in comparison to experiment and generally accepted *ab initio* methods. *Van der Wijst et al* analyzed various common DFT functional and their accuracy in determining DNA base pair hydrogen bond distances[49]. Interestingly enough, B3LYP, which is a commonly used all purpose density functional, consistently underestimated hydrogen bond length and overestimated hydrogen bond energies. BP86 was found to be one of the best functionals in that it mirrored experimental results and *ab initio* calculations using MP2[49]. It is important to have accurate approximations of

intermolecular forces because these are often what determine a pharmaceutical drug's affinity for metal-organic frameworks.

The ever improving medical industry has been fruitful in reducing the instantaneous mortality of several prevalent diseases like cancer. However, issues concerning the quality of life and efficacy of these drugs display an area of improvement in the coming years. Solutions have been proposed like macroemulsion formulations, nanoparticles delivery, and immunotherapy, but the promising, rich field of metal-organic materials as drug delivery vessels should be investigated heavily as well. Due to the endless possibilities of these structures, the field is an all-encompassing answer to various issues like poor bioavailability, adverse side effects, and low retention times of pharmaceutical drugs. Outlined by porous materials that can be used to deliver problematic pharmaceutical drugs more effectively, MOMs' facile synthesis, tunable structures, modifiable properties, and controlled release of drugs combine into an auspicious field that could be crucial in the coming years for designing less harmful patient treatments.

Discrete MOP structures showcase all of these positive attributes and do not rely upon large macroscale structures that define metal-organic frameworks. As researchers design larger metal-organic polyhedra that will outlast renal excretion due to their smaller size, their prominence as the next drug delivery vessel continues to grow. Zinc MOPs within this context have not been investigated fully and deserve more recognition as a safer metal that can exist in tetrahedral or octahedral geometries that could allow for selective synthetic methods and "smart" structures that respond to their physiological environment. This review has highlighted MOMs for their encouraging qualities, and specifically points towards the lack of research into the promising field of discrete zinc polyhedra.

Research Objectives

This project aimed to create a library of zinc metal-organic frameworks with a specific focus on applying them for pharmaceutical drug delivery. Ibuprofen was selected as the model drug due to its use in other publications, its low cost, its high solubility, and its ease of quantification. It was the goal to create a novel MOF that would uptake and release ibuprofen through a controlled rate of release. Alongside these experimental studies, computational data from a DFT analysis was planned to supplement our understanding of how ibuprofen interacts with the paddlewheel motif of AB MOF1.

Results and Discussion

A. Creating a Library of Zinc Metal Organic Materials

I aimed to create discrete zinc metal-organic polyhedra following the same structure as *Moulton et al*[39], yet replacing the copper atoms with zinc atoms. This nanoball geometry is a target for delivering our model drug, ibuprofen, for improved oral administration. I planned to conduct various reactions at room temperature and using the microwave and solvothermal methods in the oven. Various solvents like methanol, ethanol, N',N-dimethylformamide, and a series of ratios between the two were varied to generate novel structures. These solvents are utilized due to the solubility of the starting materials in these solvents and the success reported in previous literature in generating zinc MOPs[47]. A series of zinc nitrate, zinc acetate, and zinc chloride were used to study the effect of the starting material anion on the resulting MOP structures. After creating several crystal structures, some novel and others already published,

there have been no zinc MOP nanoballs created. The following results detail the creation of many distant zinc metal-organic frameworks and evaluating their efficacy for drug delivery.

Room temperature layering was not fruitful in creating crystalline products. **Table 1** details the conditions of the unsuccessful reactions with $Zn(NO_3)_2.6H_2O$ and 5-hydroxyisophthalic acid. Thus, the microwave reactor was moved to next to create possible zinc MOPs. The microwave synthesis was more successful in creating crystalline products, often making miniscule, monodisperse needles. It is believed that the zinc metal does not readily assume the octahedral geometry necessary for the nanoball structure at room temperature, which could explain the surprising lack of product from all of the room temperature reactions.

Template	Metal:Ligand Ratio	Crystal
DMSO	1:1	X
DMSO	1:2	X
DMSO	1:2.5	X
DMSO	1:3	X
DMSO	1:3.5	X
Diethyl Ether	1:1	X
Diethyl Ether	1:2	X
Diethyl Ether	1:2.5	X
Diethyl Ether	1:3	X
Diethyl Ether	1:3.5	X
Nitrobenzene	1:1	X
Nitrobenzene	1:2	X
Nitrobenzene	1:3	X

Table 1. Room temperature layering reactions ran in methanol with varying templates of DMSO, diethyl ether, and nitrobenzene. The metal to ligand ratio was modified as well, yet all of the reactions have not yielded any crystals after four months of waiting.

The microwave reactor was able to produce several products through varying the template, all of which were fine needles with the same exact morphology. When comparing the PXRD spectra of crystals formed from a 65 ^{o}C reaction for one hour in ethanol with

nitrobenzene, toluene, and 1,2 dichlorobenzene templates, it was apparent the crystals were all the same since the peaks matched up exactly. The reaction that utilized a toluene template was chosen to send off for single crystal x-ray diffraction because it had the most crystals and the best signal to noise ratio from PXRD. With large peaks present on the PXRD, this indicates that the sample is highly crystallized and ideal for single crystal characterization. Judging by the IR spectrum in **Appendix 1**, shows a splitting of the carbonyl peak at ~ 1550 cm^{-1}, which indicates the zinc metal is coordinating in a paddlewheel structure. The peaks are not completely symmetric, which may suggest that zinc could be present in the octahedral and tetrahedral geometry. Another peak of note is the prominent stretch at 1360 cm^{-1}, which is likely the N=O stretch from the nitrate anion from the zinc nitrate starting material. This peak can be observed in the IR spectra of the other products that used zinc nitrate.

Several solvothermal reactions generated large, defined crystals for x-ray diffraction analysis were at 85 ºC and 105 ºC. The following solvothermal reactions that were sent for single crystal analysis have been compiled into a table to compare their IR data (**Table 2**). Two of the structures have been published already. Their sample names will be referred to OFUYUL[50] and REHGAN[51], as this was the terminology adopted by the previous authors. It should be noted that there was no splitting of the carbonyl peak of OFUYUL, which confirms the single crystal analysis that there is no paddlewheel motif (**Appendix 3**). Again, the peak around 1360 cm^{-1} can be observed in both products' IR for the N=O stretch (**Appendix 4**). Using the first three solved samples as a benchmark, it is likely that samples ZnHIP_acetate and ZnIP both exhibit a zinc paddlewheel motif since the carbonyl peak between 1700-1600 cm^{-1} is symmetrically split. This is often an indication that the carbonyl from the dicarboxylate ligand is acting in a bridging mode and delocalizing its C=O to bind in a bidentate fashion to the metal.

Sample	Peaks on IR (cm^{-1})
REHGAN	3014.46, 1551.69, 1360.97
OFUYUL	3158.81, 1559.89, 1348.79
AB MOF1	2786.61, 1558.38, 1366.38
ZnHIP_1:1_DMF:EtOH	3264.36, 1554.46, 1348.95
ZnHIP_1:2_DMF:EtOH	3016.46, 2786.20, 2493.65, 1554.58, 1336.40, 1026.85
ZnHIP_acetate	2923.60, 2853.53, 1662.86, 1629.51
ZnIP	1599.72, 1556.39, 1391.06, 1372.75, 1346.66
ZnHIP_DMF	3351.04, 2973.37, 2788.93, 1566.48, 1339.64
ZnHIP_ZnCl	3349.77, 2912.49, 2789.32, 1567.11, 1340.30
ZnPheAdamantane	3359.56, 2879.38, 1613.60, 1573.18, 1306.68

Table 2: Table of the prominent peaks from the IR spectra of all ten samples that have been sent off for single crystal analysis (**Appendixes 2-10**).

All of the IR spectra indicate that these structures are likely not the same metal-organic materials. Comparing the PXRD of all the products this was confirmed as well (**Figure 6**). The peaks for all the products are dispersed throughout the spectra and do not overlap. The lack of overlap between the peaks confirms that these samples have a different three-dimensional morphology that is causing them to diffract light differently at separate angles of 2theta. The important take away from the three PXRD spectra in **Figure 6** is that these ten crystal structures are distinct from each other.

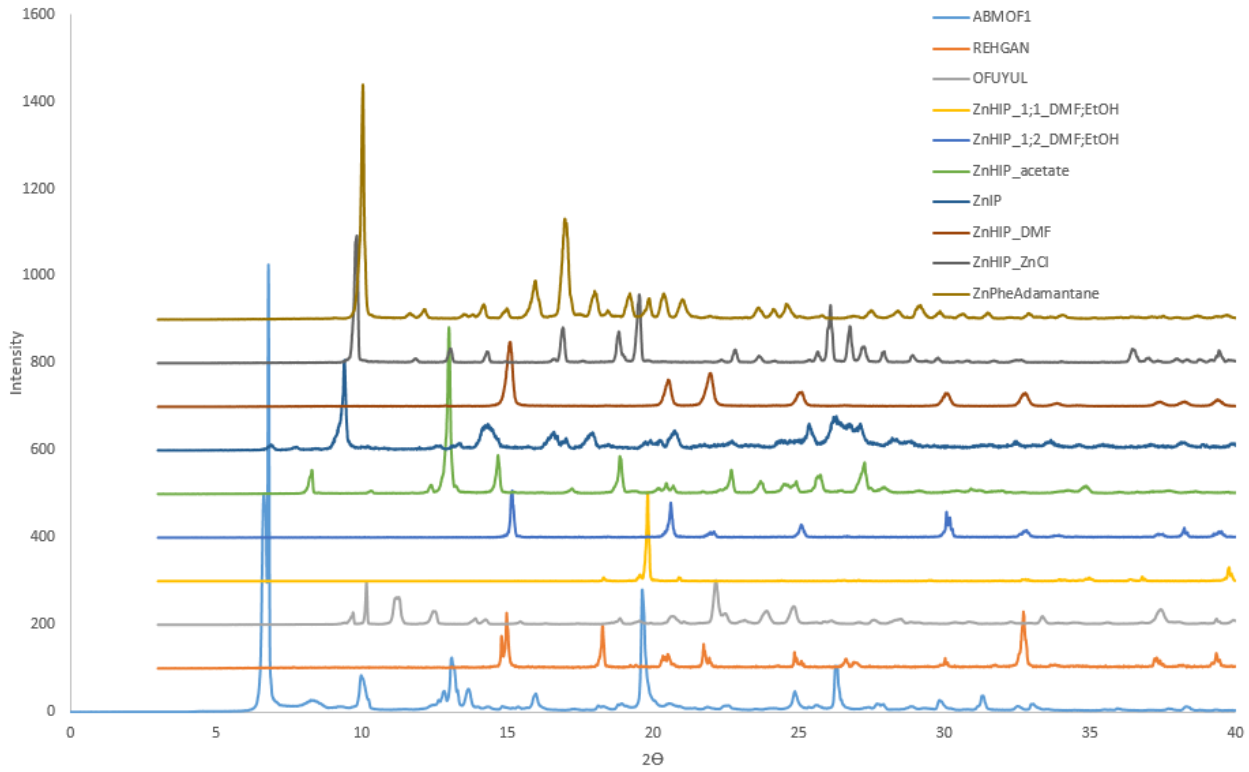

Figure 6. Powder X-ray Diffraction spectra waterfall of the ten samples that have been sent of for single crystal x-ray analysis. The incident angle (2theta) is plotted against the intensity of diffracted light.

B. Solved Structures

In sum, three crystals have been solved already by our collaborators (REHGAN, OFUYUL, and AB MOF1). These crystals have been characterized using single x-ray diffraction. Two of the three crystals have been previously reported in the literature[50,51], yet they have not investigated drug uptake applications of these frameworks. The first structure, which has been previously published as OFUYUL (catena-[bis(μ_4-5-Hydroxyisophthalato)-di-zinc(ii) unknown solvate monohydrate]) exhibits zinc in a tetrahedral geometry binding to every oxygen present on the 5-hydroxyisopthalate ligand[50]. This creates an irregular lattice with misshapen

square pores present, and zinc binds also to aqua ligands along with the 5HIP organic ligand (**Figure 7**).

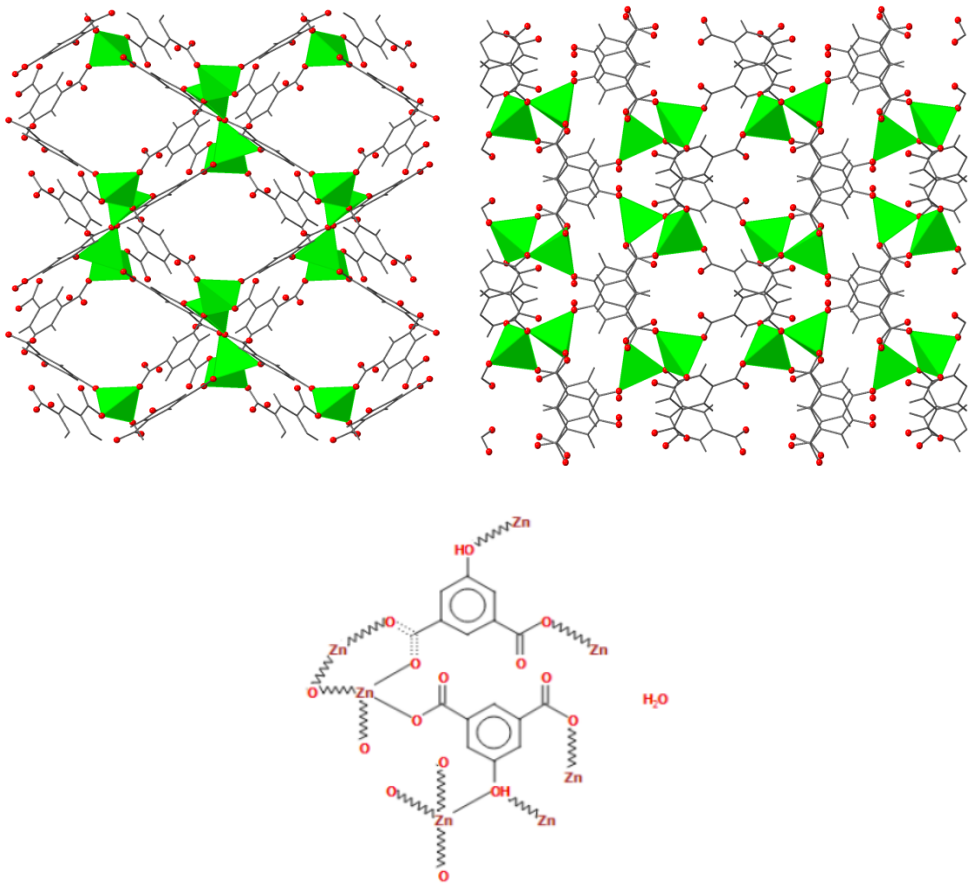

Figure 7: (left) unit cell of OFUYUL viewed from the a axis, (right) unit cell of OFUYUL from c axis, and (below) lewis structure of OFUYUL repeating unit.

REHGAN[51] [catena-((μ_2-5-Hydroxyisophthalato-O,O')-triaqua-zinc(ii))] (**Figure 8**) exhibits an entirely different morphology from OFUYUL, yet zinc behaves in a very similar way. The zinc atom binds to three aqua ligands except that a zinc atom does not bridge the 5-hydroxyisophthalate ligands together like in AB_MOF1 (**Figure 9**). Thus, while OFUYUL is a polymeric three dimensional lattice held together by covalent bonds, REHGAN is a repeating 5-

hydroxyisophthalate unit held together by π-π stacking from the benzene rings of the organic ligand.

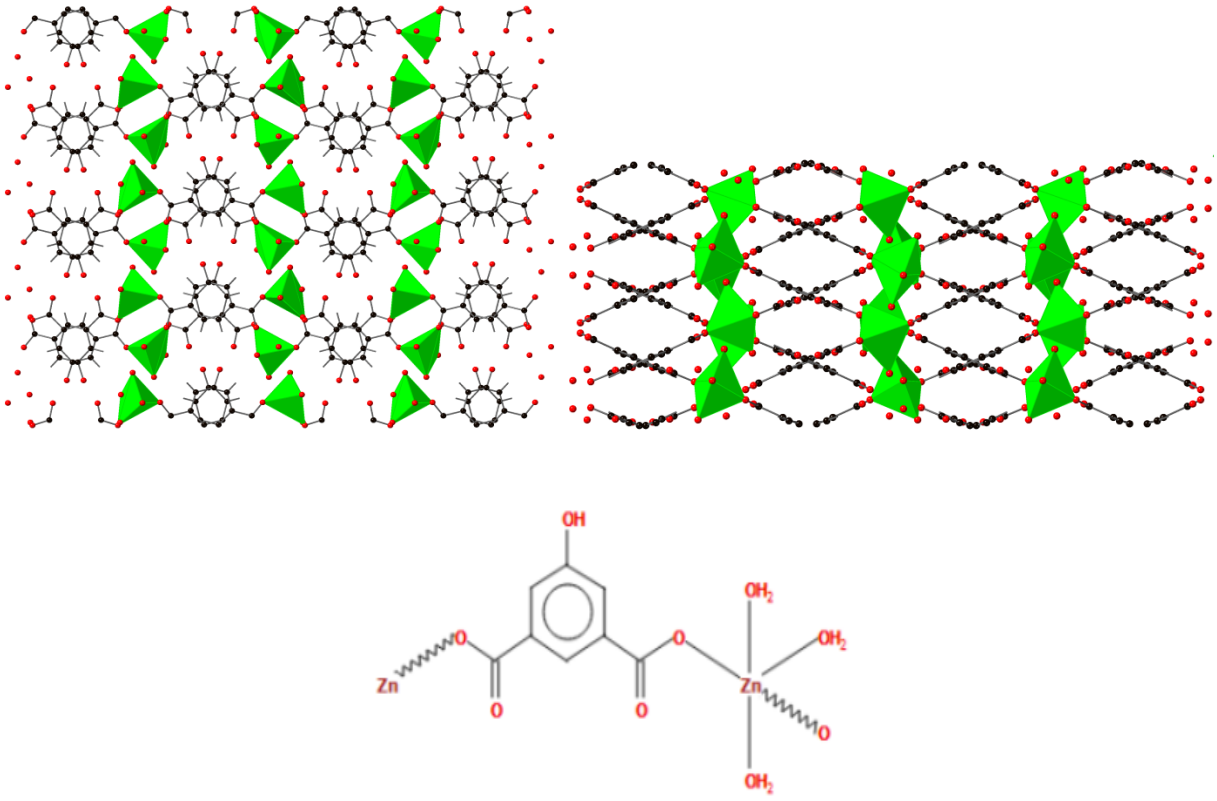

Figure 8: (left) single crystal structure of REHGAN's unit cell visualized from the b axis, (right) unit cell of REHGAN seen from the c axis, and (below) lewis structure of the repeating unit in REHGAN.

The final structure characterized, AB MOF1, reflects closely to the nanoball from *Moulton et al*. The desired zinc paddlewheel structure was attained, yet instead of having the 5-hydroxyisophthalate ligands all turn inwards to enclose the structure into a nanoball, they flip-flop across the paddlewheel in a trans fashion (**Figure 9**). Even the axially bonded ethanol ligands point in opposite directions from each other on the crystal structure. This could be occuring since the system is trying to reduce steric interaction and consequently directs all of the

bulky 5-hydroxyisopthalate ligands away from each other to reduce steric strain. Another interesting observation is the presence of two equivalents of 2,6 dimethylpyridine base in the centroid cavity of the MOF. This was not expected and it is theorized that this could have acted as a template for the MOF to construct itself.

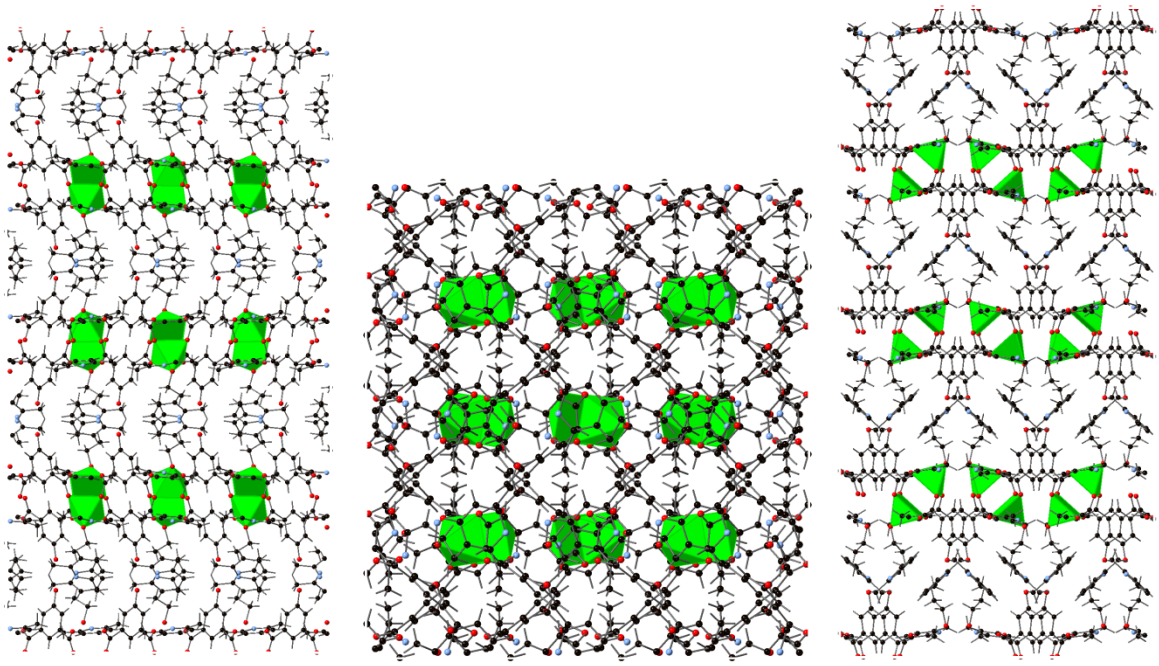

Figure 9: Three dimensional structure of AB MOF1. It creates a two dimensional sheet that through intermolecular attractive forces stacks on top of each other to create a pseudo three dimensional lattice. The two equivalents of lutidine base as shown in the center of each semi-square cavity of the MOF. From left to right the axis views are from a, c, and b perspectives respectively.

Although the desired zinc 5-hydroxyisophthalate nanoball was not successfully created as hypothesized, the three structures that have been synthesized do show promise for uptake of ibuprofen. The structure that is exceptionally promising is the novel AB MOF1 that exhibits high repetitive symmetry that will allow for easy computational modeling. Additionally, the hydroxyl groups of the 5HIP ligand jut out into the pores of the two dimensional sheet and provide a

"hook" that ibuprofen can attach to through intermolecular forces and have an increased affinity towards. This theory is supported by the fact that 2, 6 dimethylpyridine occupies the pore spaces between 2D sheets, and the nitrogen of 2, 6 dimethylpyridine orients itself towards the hydroxide group from 5-hydroxyisophtalic acid. This hydrogen bonding interaction is what we have identified is the likely area for ibuprofen to interact as well.

C. Stability Studies

Before ibuprofen uptake was evaluated, it was important to understand the stability of AB MOF1 in various solvents, especially solvents that resemble biological systems. AB MOF1 was solvated in ethanol, methanol, and water, and it was monitored for 18 hours using Powder X-ray Diffraction (PXRD) to determine how various solvents changed the three dimension morphology of AB MOF1. This was paired with IR spectroscopy and Raman, but Raman spectroscopy did not yield strong enough peak intensities for proper analysis. This was likely due to the naturally low amount of Raman scattering that occurs, which was overshadowed by the solvent O-H peaks from methanol and ethanol. When looking at the PXRDs of AB MOF1 in ethanol, methanol, and water, it is apparent that AB MOF1 is the most stable in ethanol since the spectra does not differ widely from the PXRD of AB MOF1 dried, and the spectrum does not shift as time progresses. This should make intuitive sense since AB MOF1 was synthesized in ethanol, so it should be the most stable in its mother solution (**Figure 10**).

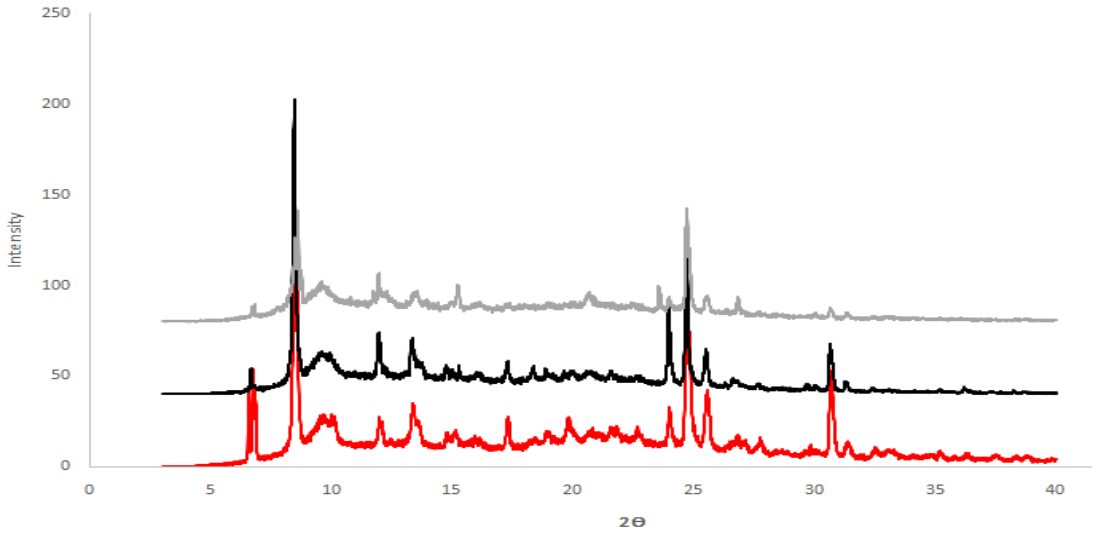

Figure 10: Comparison of AB MOF1 solvated in ethanol for 1 hour (red), 2 hours (black), and 18 hours (gray).

As expected, AB MOF1 was not as stable in methanol. Methanol is more polar and a harder Lewis base than ethanol, so it is expected that methanol will outcompete the terminally ligated ethanol molecules present on AB MOF1s paddlewheel. The PXRD mirrors this notion, and AB MOF1 quickly degrades and changes morphology when solvated in methanol (**Figure 13**). There are many hypotheses that could cause this, but again this is likely due to the competition of ethanol and zinc for the terminal ligand position to zinc, and this sterically misshapes AB MOF1 into a different morphology. The disappearance of the peak at 5 and peaks after 30 2Θ at 18 hours shows a changed structure. Additionally, the broadening of the peaks in comparison to AB MOF1 dried shows that there is likely more amorphous crystal material present.

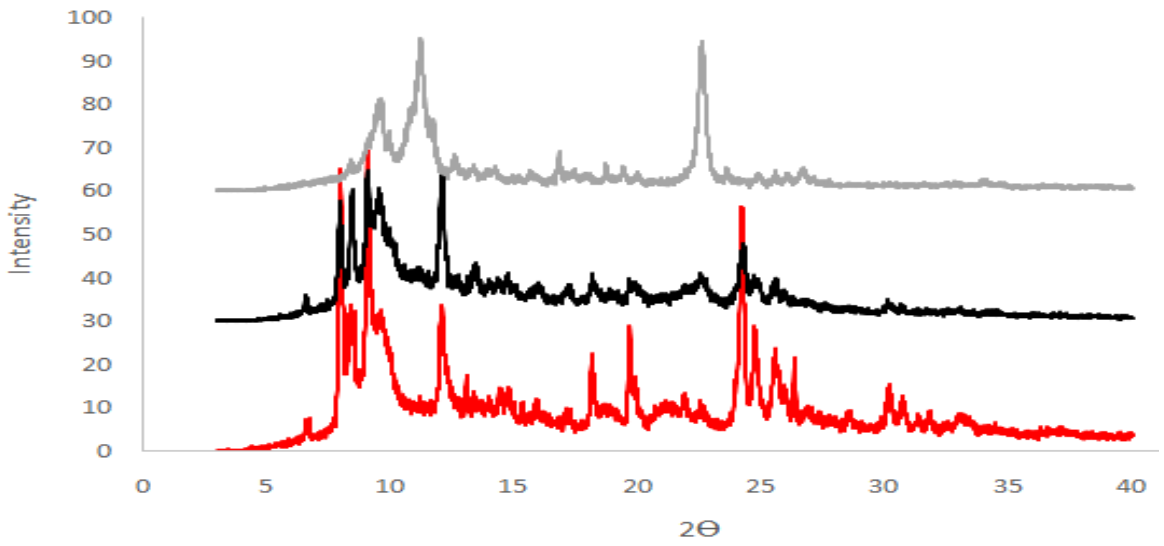

Figure 11: PXRD spectra of AB MOF1 in methanol for 1 hour (red), 2 hours (black), and 18 hours (grey).

A surprising discovery was the stability of AB MOF1 in water. If the same reasoning that was used for methanol applies to water, then AB MOF1 should be even less stable in water since water is so polar. However, AB MOF1 is astoundingly stable in water (**Figure 12**). Historically, zinc MOFs are not stable in water and can degrade upon just the smallest amount of moisture in the air (MOF1 for example). When comparing the PXRD for AB MOF1 in water, the peaks do not broaden or disappear, and they match up well with the dried AB MOF1 product. This indicates that AB MOF1 is fairly stable in water. This shows the promise of using AB MOF1 in biological applications since most of the body is composed of water.

Normally zinc and water are extremely attracted to each other since water is a hard Lewis base and zinc is a hard Lewis acid. The affinity zinc has for water is reflected in OFUYUL and REHGAN zinc MOFs where there are several aqua ligands present on zinc. What is perplexing then is why AB MOF1 prevents water from exchanging with the other ligands. A hypothesis on why this occurs is that water is too polar to enter the highly hydrophobic environment of AB

MOF1 – the π- π stacking of 2, 6 dimethylpyridine and 5-hydroxyisopthalic acid would be disrupted, so water does not enter.

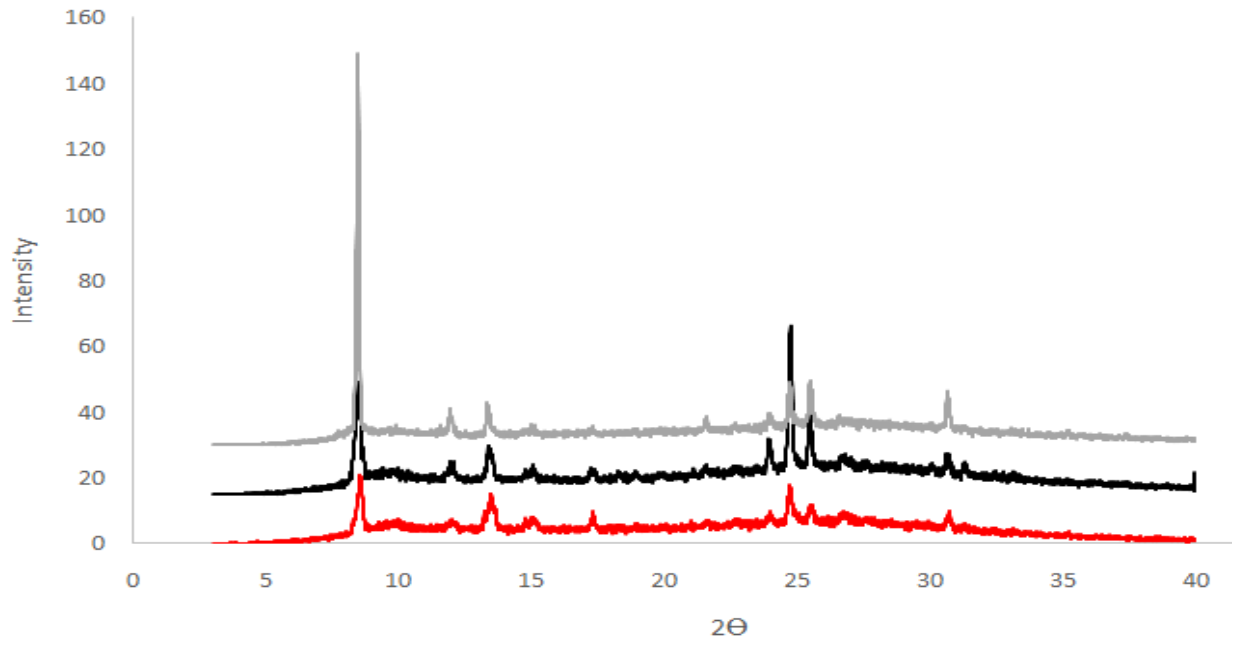

Figure 12: PXRD of AB MOF1 in water after 1 hour (red), 2 hours (black), and 18 hours (grey).

D. AB MOF1 Ibuprofen Uptake

Ibuprofen uptake studies were conducted similar to *Horcajada et al*[17], which are described in detail in the methods section. Thermal Gravimetric Analysis (TGA) was conducted of all of the ibuprofen impregnated AB MOF1 samples that were stirred in the ibuprofen solution for 1 hour, 14 hours, and 42 hours. Ibuprofen's boiling point is at 157 ºC, and it is apparent in **Figure 13** that there is a steep descent in Weight (%) at ~ 150 ºC which would correspond to ibuprofen being released from the structure. The change in Weight (%) for when ibuprofen evaporated from the sample was used to extrapolate how much ibuprofen was absorbed by AB MOF1.

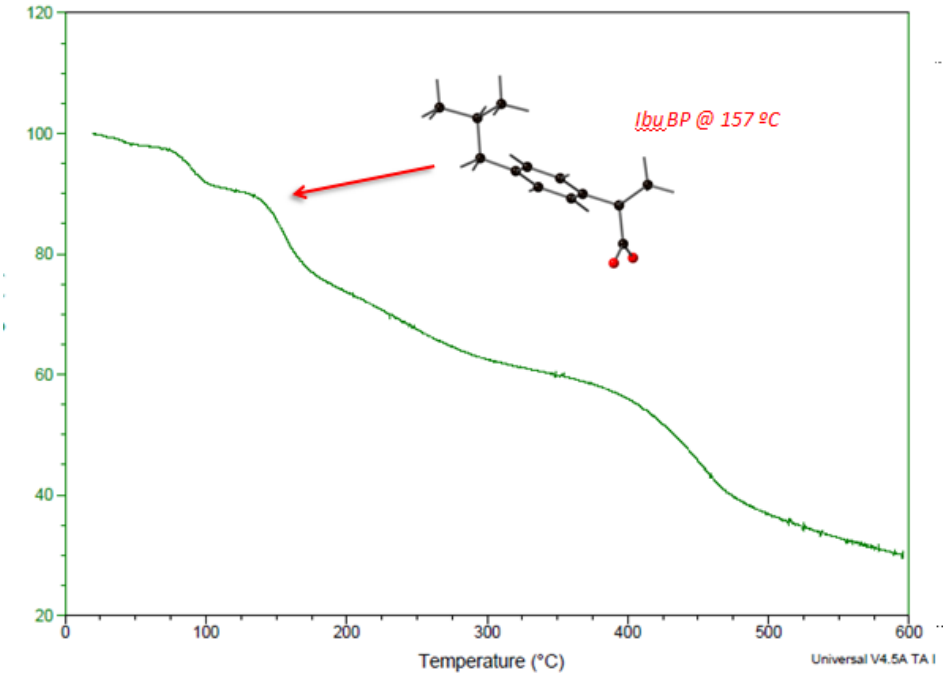

Figure 13: Thermal Gravimetric Analysis of AB MOF1 impregnated with ibuprofen for 1 hour. The bp of ibuprofen is shown with an arrow on the graph where its evaporation from AB MOF1 begins.

The amount of ibuprofen absorbed was then plotted on a graph versus the time of stirring in the ibuprofen solution (**Figure 14**). What can be noted from **Figure 14** is that the amount of ibuprofen uptake per AB MOF1 plateaus considerably after 14 hours. The values of 14 hours and 48 hours are almost identical. There are many theories for this, but the likely answer is that AB MOF1 has reached its capacity for ibuprofen shortly after half a day. However, there were issues with AB MOF1 slowly dissolving in the ibuprofen/ethanol solution over long periods of time, which prevented stirring for more than 48 hours before the sample was completely solubilized in solution. This could have had an impact on the amount of ibuprofen absorbed for longer periods of time. Nonetheless, the ibuprofen uptake of AB MOF1 is comparable to the result obtained by *Horcajada et al*[17] for MIL 53. They obtained .104 g of ibuprofen/ g of MOF absorbed after 1 day of stirring, and AB MOF 1 absorbed .107 g of ibuprofen / g of MOF after 14 hours of stirring.

This data is exciting and shows the promising and showcases the promise of AB MOF 1 for drug delivery.

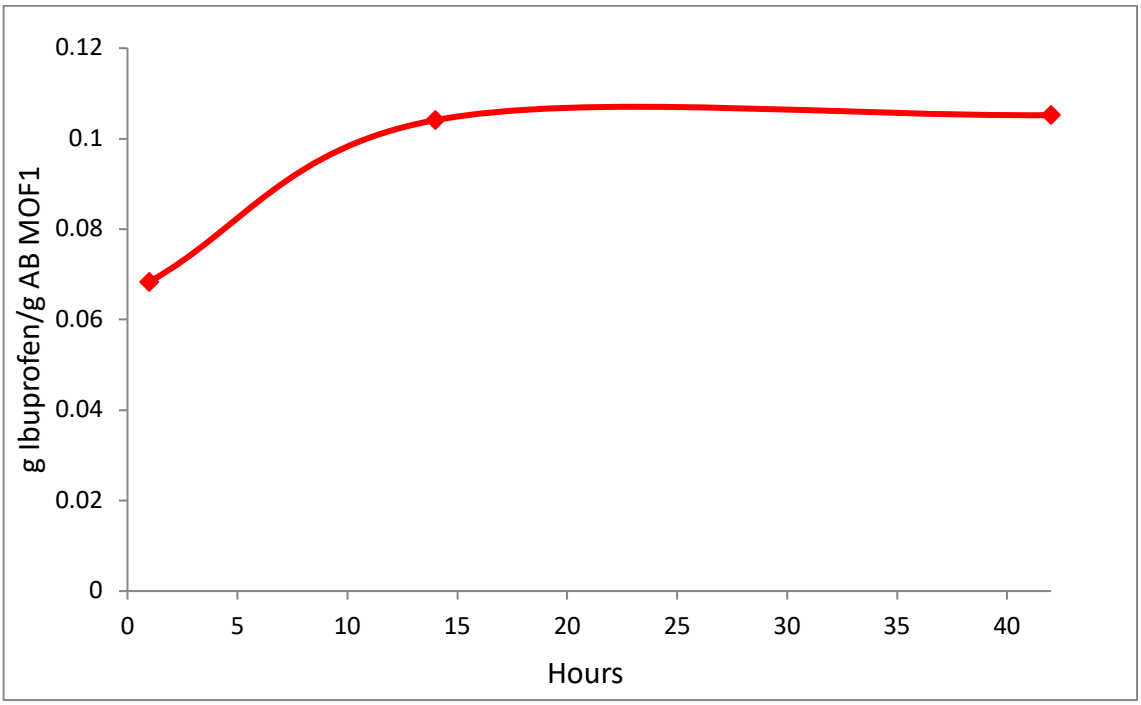

Figure 14: Graph of ibuprofen uptake by AB MOF1 plotted over time which was determined through TGA.

PXRD additionally confirms that ibuprofen was absorbed into AB MOF1. When looking at **Figure 15**, one can notice that dried AB MOF1 and the PXRD from AB MOF1 impregnated with ibuprofen differ considerably. The absence of a peak around a 2Θ of 7 in the AB MOF1-Ibuprofen sample and the addition of peaks elsewhere in the spectra is a solid indication that the three dimensional morphology of AB MOF1 is changing when ibuprofen is introduced. Thus TGA confirmed that ibuprofen was present in the sample, and then PXRD showed that ibuprofen was integrated into the sample such that it changed the overall structure of AB MOF1.

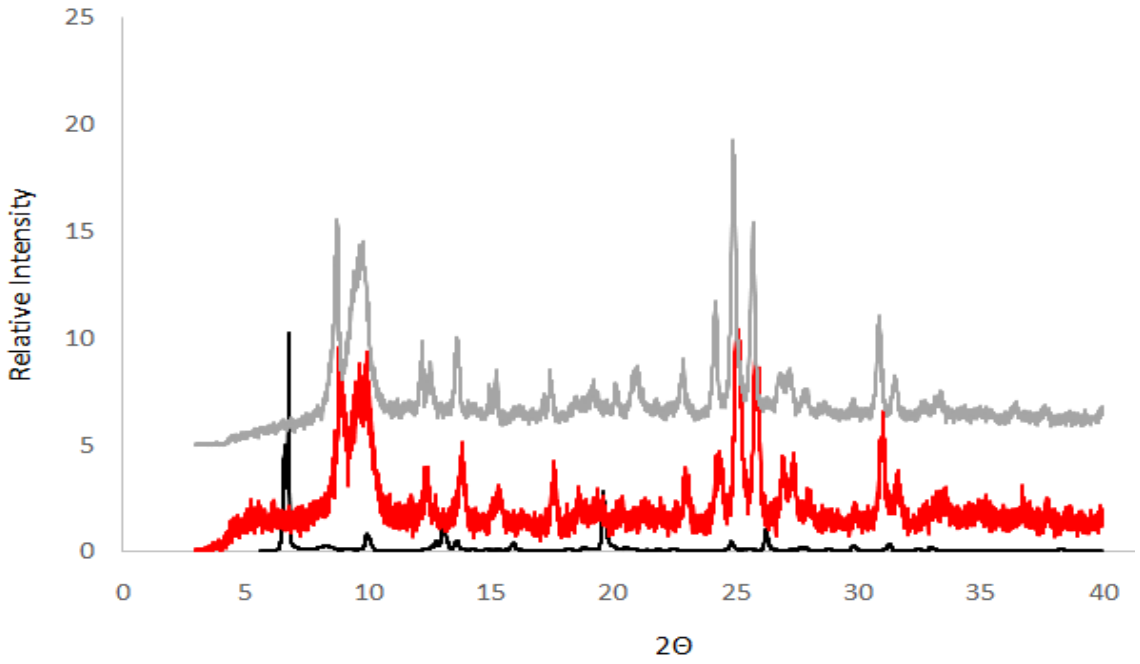

Figure 15: PXRD waterfall of AB MOF1 dried (black), AB MOF1 impregnated with ibuprofen for one hour (red), and AB MOF1 impregnated with ibuprofen for 42 hours (grey).

E. DFT Study – Interaction Energy

Density Functional Theory was used in conjunction with experimental characterization to understand the method of binding for the model compound ibuprofen. In order to achieve this, the copper nanoball structure reported by *Moulton et al*[38] was calculated for its optimum geometry and energy. However, since the nanoball is too large and cumbersome for DFT calculations, we reduced the calculation to one copper paddlewheel unit of two copper atoms and four organic ligands. This paddlewheel is repeated twelve times throughout the structure and has high symmetry. Following this, the optimum geometry and energy of ibuprofen was simulated as well. Then, the hydrogen bonding affinity was determined by simulating ibuprofen within hydrogen bonding range of the paddlewheel (where energy of interaction = |[ibuprofen alone + paddlewheel alone] - (ibuprofen and paddlewheel)|). This is defined as a relative energy value divided by the total energy of the complex. A “favorable” interaction is defined as binary, simply

having a lesser energy of ibuprofen and the paddlewheel together will show a favorable interaction. This is all detailed in **Figure 16** that shows the scheme for determining the energy of interaction between the MOF and ibuprofen. This was done for both the copper nanoball by *Moulton et al*[38] and AB MOF1. The carboxylic acid moiety of ibuprofen was simulated within hydrogen bonding range to the hydroxyl group of 5-hydroxyisopthalic acid (~ 2 Angstroms). This energy of interaction was defined as a low-ball estimate of the actual energy of interaction because only a single point energy calculation was run, and ibuprofen was moved by hand in a pseudo-geometry optimization. Since we were not able to conduct a full geometry optimization due to computational limitations, the estimated energy of interaction shown in **Figure 16** is absolutely larger than calculated. The energy of interaction value of ~ 1 kcal/mol is comparable to the experimentally defined hydrogen bond, which is on the order of 1-5 kcal/mol[49], which indicates our methodology was sound and calculated the energy of interaction within the correct order of magnitude.

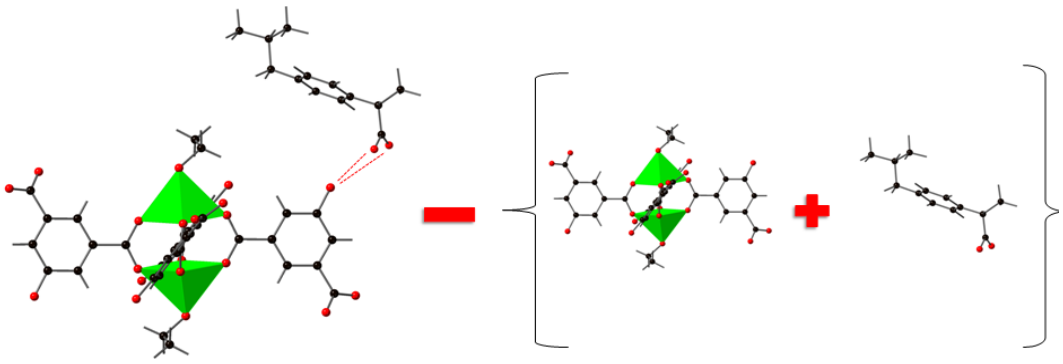

Figure 16: Scheme showing how the energy of interaction is defined through the single point energy calculation of the AB MOF1 paddlewheel with ibuprofen subtracted by separate single point energy calculations of AB MOF1 and ibuprofen separate.

F. Electron Microscopy of AB MOF1

Scanning Electron Microscopy (SEM) and Transmission Electron Microscopy (TEM) were used in conjunction with other characterization methods to better ascertain how ibuprofen is interacting with AB MOF1. TEM (**Figure 17**) showed that AB MOF1-Ibuprofen assumes various three dimensional geometries. There are cubic, rectangular, and amorphous structures that are present throughout the sample, ranging from under 100 nm to up to a micron in size. It is difficult to make any conclusions regarding the uptake of ibuprofen within the structure since the resolution is so low. The surface of AB MOF1-Ibuprofen can be viewed using Scanning Electron Microscopy (SEM) (**Figure 18**), where there are several invaginations throughout the surface. On top of these negative impressions in the surface, there are also projections that jut out into space – both of which contribute to increasing the surface area of AB MOF1. Unfortunately since the control AB MOF1 with no ibuprofen has not been imaged using electron microscopy due to time constraints, it is difficult to make any clear assertions about ibuprofen binding when just viewing AB MOF1-Ibuprofen alone.

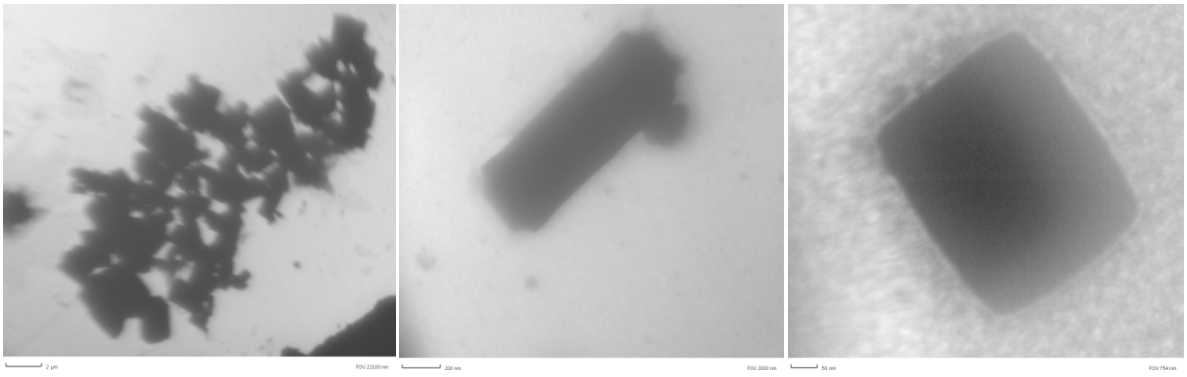

Figure 17: Transmission Electron Microscopy (TEM) images of AB MOF1-Ibuprofen.

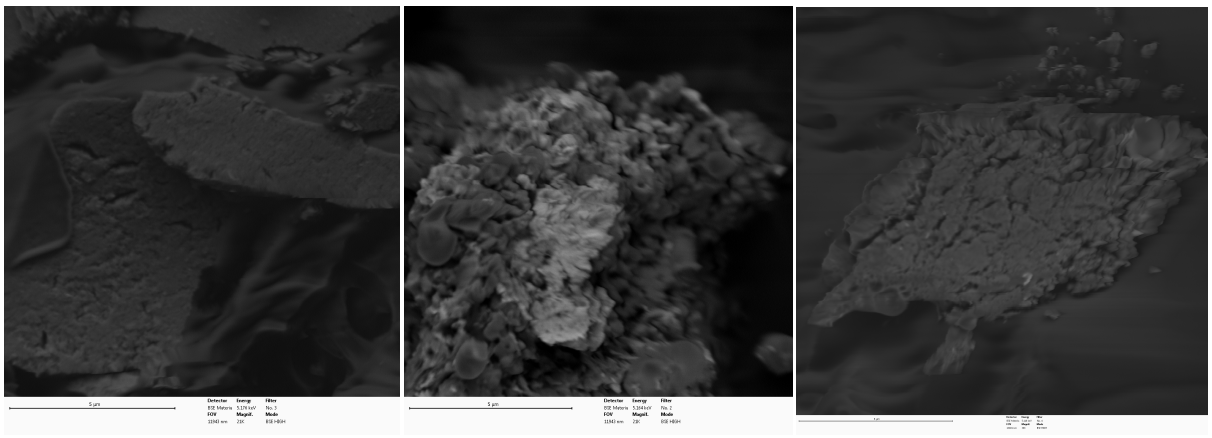

Figure 18: Scanning Electron Microscopy (SEM) of AB MOF1 impregnated with ibuprofen.

Conclusion

In sum, a library of zinc metal-organic frameworks have been successfully created and characterized. A total of ten samples of zinc MOFs have been sent to single crystal analysis, and three have been solved currently. Of those three one was a novel MOF – AB MOF1. AB MOF1 was evaluated for its use in drug delivery by using the model pharmaceutical drug ibuprofen for uptake studies. AB MOF1's stability in various common solvents like ethanol, methanol, and water was monitored using PXRD, which gave insights on its crystallinity and three dimensional structure over time. AB MOF1 was the most stable in ethanol, but it was surprisingly stable in water for a zinc MOF, which are notoriously unstable in the presence of water. This could be attributed to the π-π stacking of the 2, 6 dimethylpyridine base and 5-hydroxyisophtalate in AB MOF1, which would prevent the polar water from entering inside the structure to exchange with the ligands of AB MOF1. In future work, it will be pertinent to look into the stability of AB MOF1 in varying pHs, specifically acidic conditions if it is to be used for oral absorption.

The ibuprofen uptake of AB MOF1 was deemed successful through subsequent characterization of AB MOF1-Ibuprofen impregnated pellets using TGA and PXRD. The

evaporation of ibuprofen at 157 ºC along with the change in morphology of AB MOF1 from PXRD give a likely indication ibuprofen was absorbed into AB MOF1. The percent change in the sample was used to extrapolate the uptake of AB MOF1, which reached capacity of ibuprofen uptake after 14 hours. The uptake of ibuprofen is comparable to the data reported by *Horcajada et al*[17], who obtained 0.104 g of ibuprofen/ g of MOF after one day of stirring while AB MOF1 obtained 0.107 g of ibuprofen/ g of MOF after 14 hours of stirring. Further tests will need to troubleshoot the durability of AB MOF1 pellets and create a better uptake procedure to ensure AB MOF1 does not dissolve in solution over extended periods of stirring. Additionally, future work will look into the rate of release of ibuprofen by AB MOF1 after it has been impregnated. This will be done through UV-Vis and HPLC to determine the concentration of ibuprofen in the solution.

Computational DFT studies corroborate the fact that the interaction between ibuprofen and AB MOF1 is favorable. The functionalized pore of AB MOF1 serves as an anchor for polar compounds, specifically the hydroxyl group of the 5-hydroxyisophtalate ligand was determined to be a possible site of interaction for the carboxylic acid moiety of ibuprofen. The energy of interaction between the zinc paddlewheel motif and ibuprofen was calculated to be 1.030 kcal/mol, which is on the same order of magnitude for the energy of a hydrogen bond. Future studies will conduct more manual single point energy calculations to determine the optimal distance for ibuprofen in relation to the zinc paddlewheel structure.

Methodology

Room Temperature Layering 1 mmol of zinc nitrate hexahydrate was added to 5 mL of solvent (solvent consisted of methanol, N, N-dimethylformamide, or a ratio of the two from 1:3 EtOH:DMF to 3:1 EtOH:DMF). 1 mmol of 5-hydroxyisopthalic acid was added and stirred until completely dissolved. Then, 2.2 mol of 2,6 dimethylpyridine was added and dissolved. This 5-hydroxyisopthalic acid solution was then added slowly on top of the layering template (template used was DMSO, diethyl ether, or nitrobenzene). When the metal:ligand ratio was modified, the amount of 2,6 dimethylpyridine was changed accordingly to be ~2.2 equivalents more than the organic ligand.

Microwave Reactions 1 mmol of zinc nitrate hexahydrate was added to 5 mL of solvent (solvent consisted of ethanol or N, N-dimethylformamide). 1 mmol of 5-hydroxyisopthalic acid was added and stirred until completely dissolved. Then, 2.2 mol of 2,6 dimethylpyridine was added and stirred for 30 min. This 5-hydroxyisopthalic acid solution was then added slowly on top of 625 microliters of the layering template (templates used were nitrobenzene, 1,2 dichlorobenzene, or toluene). When the metal:ligand ratio was modified, the amount of 2,6 dimethylpyridine was changed accordingly to be ~2.2 equivalents more than the organic ligand. The reaction was put in the microwave reactor and set at various temperatures (65, 85, and 105 ^{o}C) for 1 hour each run.

Solvothermal Reactions: 1 mmol of zinc starting material (either zinc nitrate hexahydrate, zinc acetate, or zinc chloride) was added to 5 mL of solvent (solvent consisted of ethanol or N, N-dimethylformamide, or a ratio of the two from 1:3 EtOH:DMF to 3:1 EtOH:DMF). 1 mmol of 5-

hydroxyisopthalic acid was added and stirred until completely dissolved. Then, 2.2 mol of 2,6 dimethylpyridine was added and stirred for 30 min. This 5-hydroxyisopthalic acid solution was then added slowly on top of 625 microliters of toluene. When the metal:ligand ratio was modified, the amount of 2,6 dimethylpyridine was changed accordingly to be ~2.2 equivalents more than the organic ligand. The reaction was put in the microwave reactor and set at various temperatures (85, and 105 ºC) for varying times ranging from 48 to 120 hours.

Determination of MOF Stability: The metal organic framework was added to a series of different solvents (methanol, ethanol, and water). The solid that was still present in solution was taken out of solution and then analyzed via Powder X-ray Diffraction. Infrared spectroscopy spectra were taken of the samples as well. This was done at three separate times to monitor the change in AB MOF1 over the course of eighteen hours (1, 2, and 18 hrs were when the samples were analyzed).

Ibuprofen Uptake: Ibuprofen uptake studies followed the methodology reported by *Horcajada et al*[17], where the MOFs were pressed into a pellet and then added to a solution of ibuprofen. The ibuprofen solution was 30 g/L in ethanol solvent. The ibuprofen-MOF solution was stirred for varying amounts of time (1, 2, 24, and 48 hrs) and their ibuprofen uptake was determined with thermal gravimetric analysis (TGA). The change in mass at 157 ºC was designated as the ibuprofen release due to ibuprofen's boiling point at 157 ºC, so the percent change was evaluated at that temperature.

Computational Methods: The copper nanoball reported by *Moulten et al*[39] was of first interest. A copper paddlewheel motif that is repeated 12 times in the structure was simulated due to the overwhelming size of the whole copper nanoball for density functional theory Gaussian methods using the software package nwchem. Geometry optimizations and then single point energies were run on the copper paddlewheel unit using first a BP86 functional with a sto-3g basis set and an AE1 basis set. The AE1 basis set[44] assigns a Watchers basis set for the copper atom and a 6-31g* basis set for the carbon, hydrogen, and oxygen atoms. Geometry optimizations and single point energies were then run on ibuprofen using the BP86 functional with a 6-31g* basis set. Ibuprofen and the copper paddlewheel motif were then superimposed upon each other to simulate the interaction between the two. The hydrogen bonding interaction between the carboxylic functional group and the 5-hydroxyl group of the 5HIP ligand was determined to be a favorable site for interaction. Thus, energies from the copper paddlewheel alone and ibuprofen alone were summed and subtracted from the energy of ibuprofen with the copper paddlewheel. This relative difference in energy was defined as the energy of interaction. For AB MOF1 Gaussian was utilized instead of nwchem, and BP96 functional with a Watcher's basis set for Zn was used. However, the other atoms were assigned a 6-311+g basis set instead. The same procedure described previously for determining the energy of interaction was used again.

Appendix

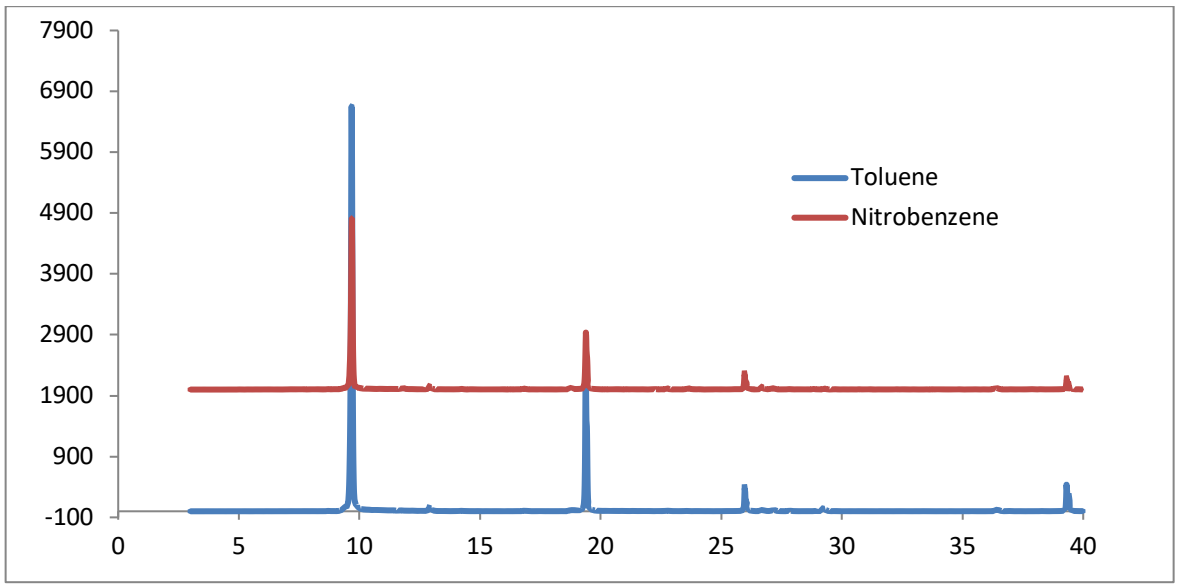

Appendix 1: PXRD spectra of microwave reactions of zinc nitrate and 5-hydroxyisopthalic acid at 65 C. The blue spectrum represents the reaction done with a toluene template, and the red one is for the nitrobenzene template.

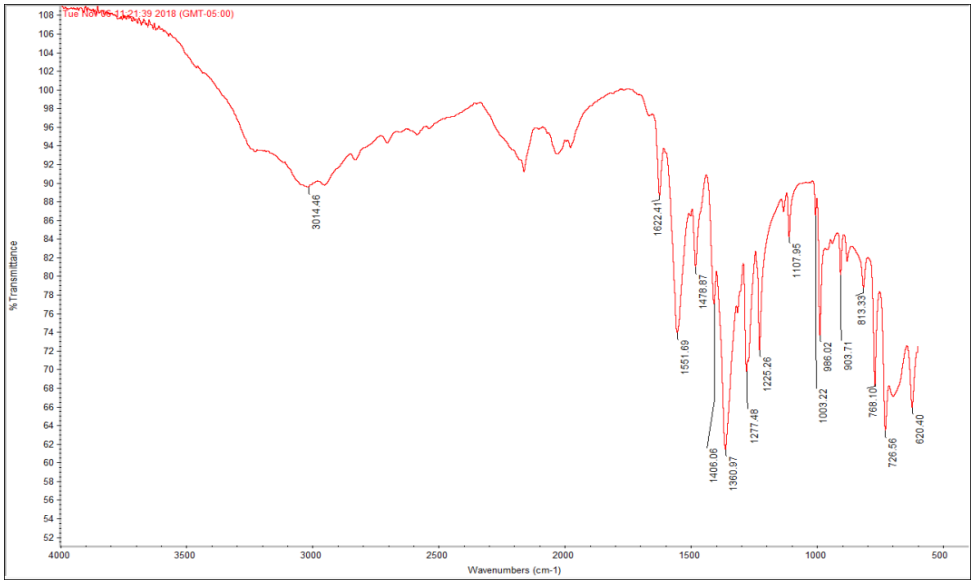

Appendix 2. Infrared absorption spectrum of zinc 5-hydroxyisophthalate product formed via microwave reaction using a toluene template. Prominent peaks are 3014.46, 1551.69, and 1360.97 cm^{-1}.

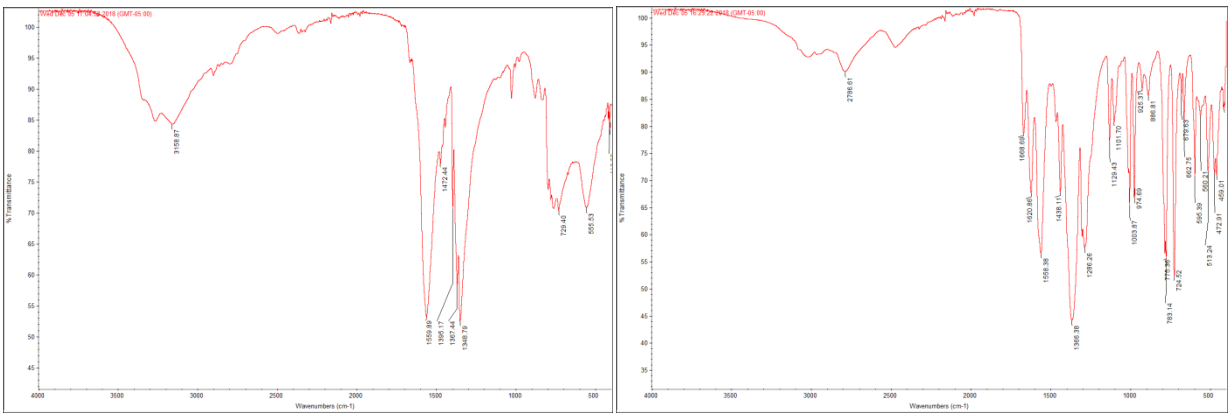

Appendix 3. IR spectra of REHGAN (*left*) and OFUYUL (*right*) products. Prominent peaks for REGHAN are 3158.81, 1559.89, 1348.79 cm^{-1}. Prominent peaks for OFUYUL are 2786.61, 1558.38, 1366.38 cm^{-1}.

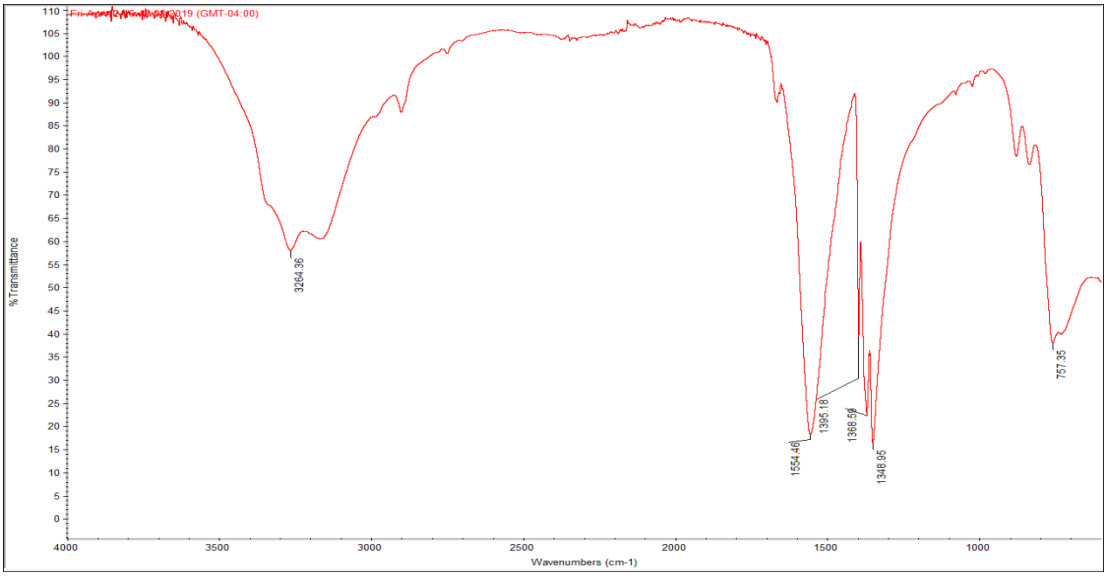

Appendix 4: IR spectra for ZnHIP_1:1_DMF:EtOH. Prominent peaks can be observed at 3264.36, 1554.46, 1348.95 cm^{-1}.

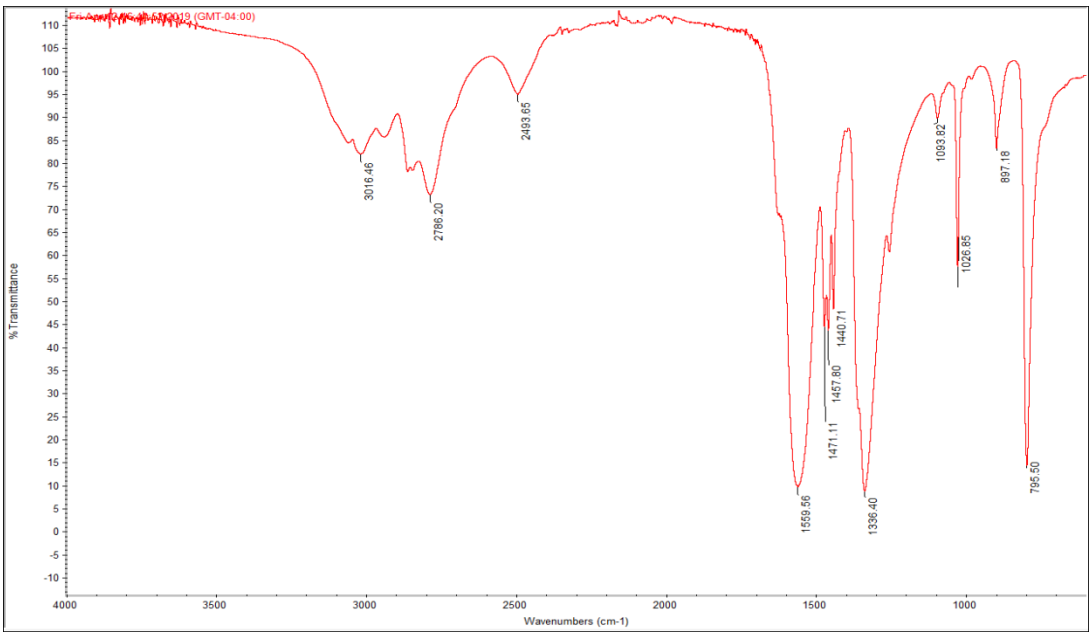

Appendix 5: IR spectra for ZnHIP_1:2_DMF:EtOH. Prominent peaks can be observed at 3016.46, 2786.20, 2493.65, 1554.58, 1336.40, 1026.85 cm^{-1}.

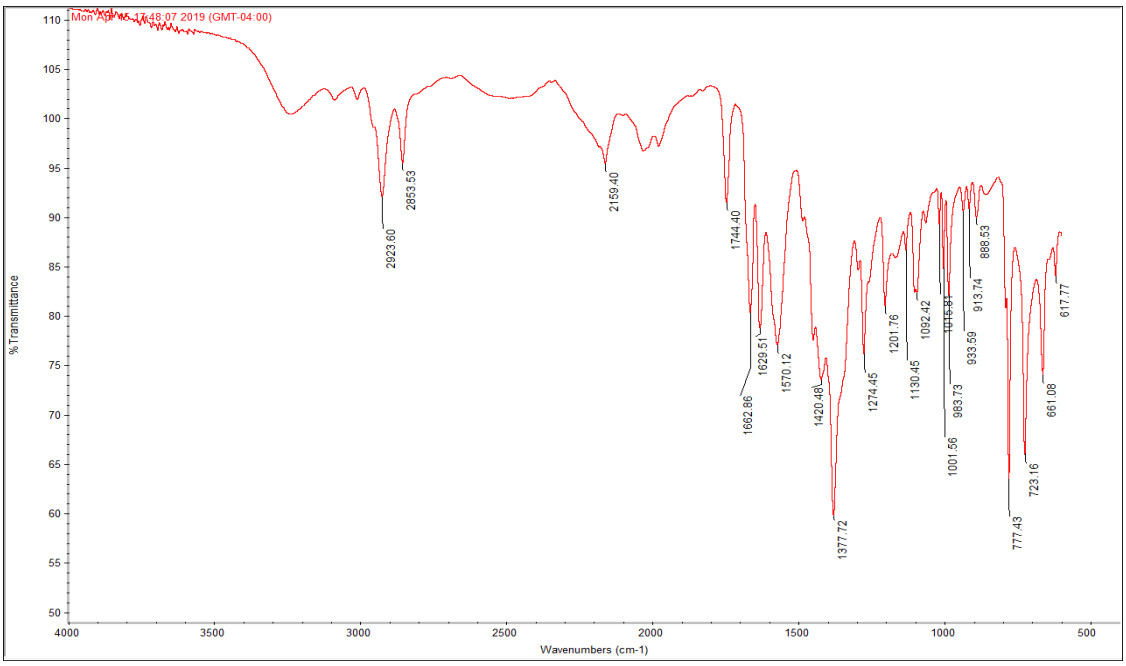

Appendix 6: IR spectra for ZnHIP_acetate. Prominent peaks can be observed at 2923.60, 2853.53, 1662.86, 1629.51 cm^{-1}.

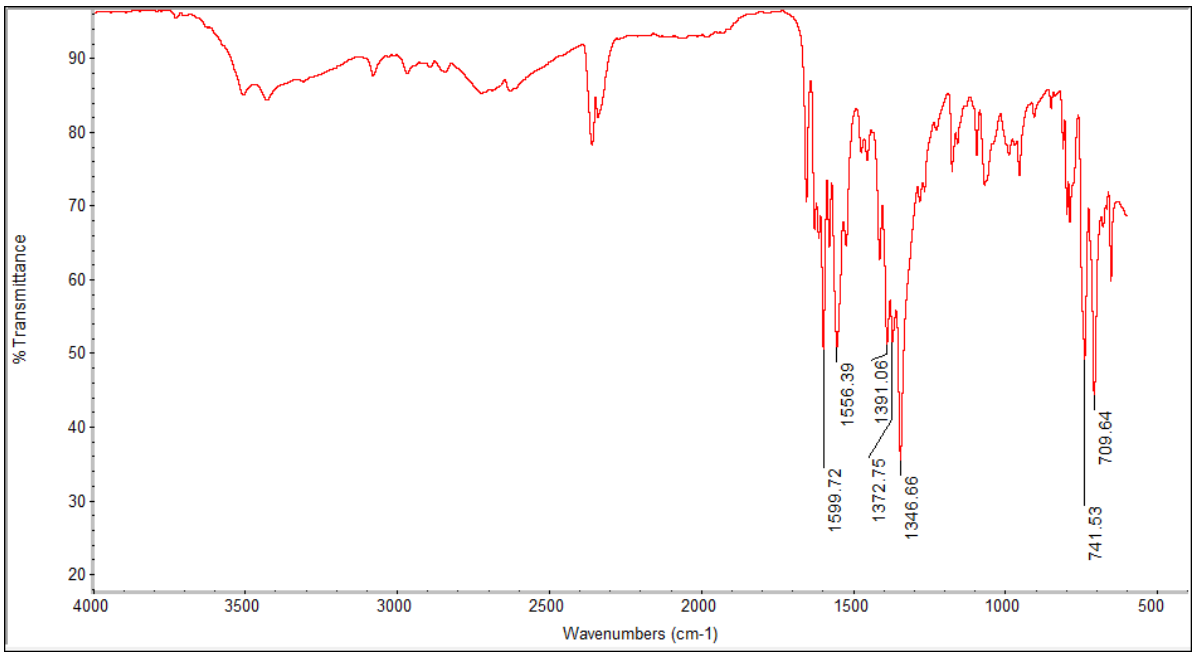

Appendix 7: IR spectra for ZnIP. Prominent peaks can be observed at 1599.72, 1556.39, 1391.06, 1372.75, 1346.66 cm^{-1}.

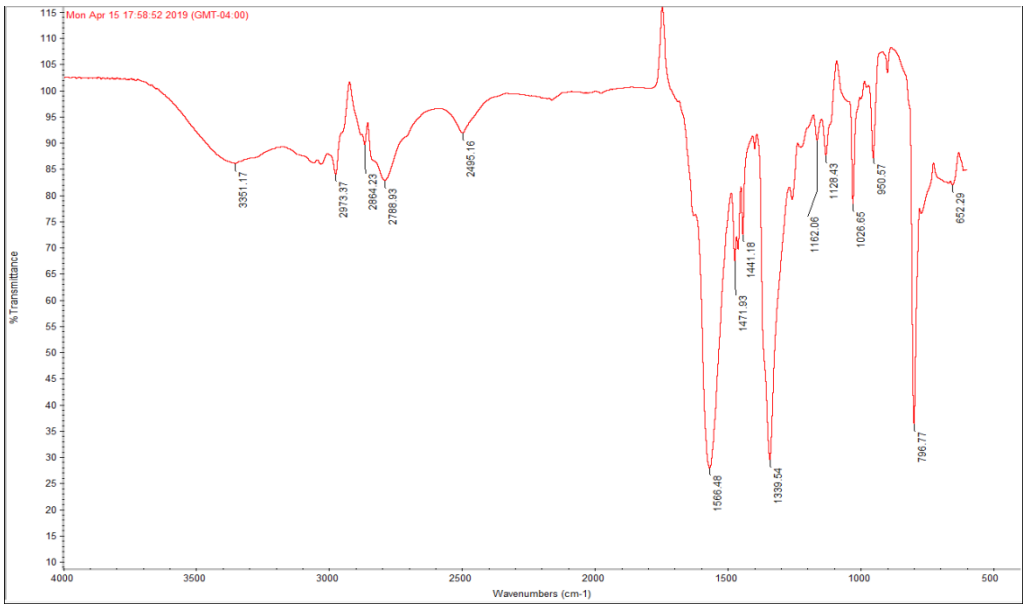

Appendix 8: IR spectra for ZnHIP_DMF. Prominent peaks can be observed at 3351.04, 2973.37, 2788.93, 1566.48, 1339.64 cm^{-1}.

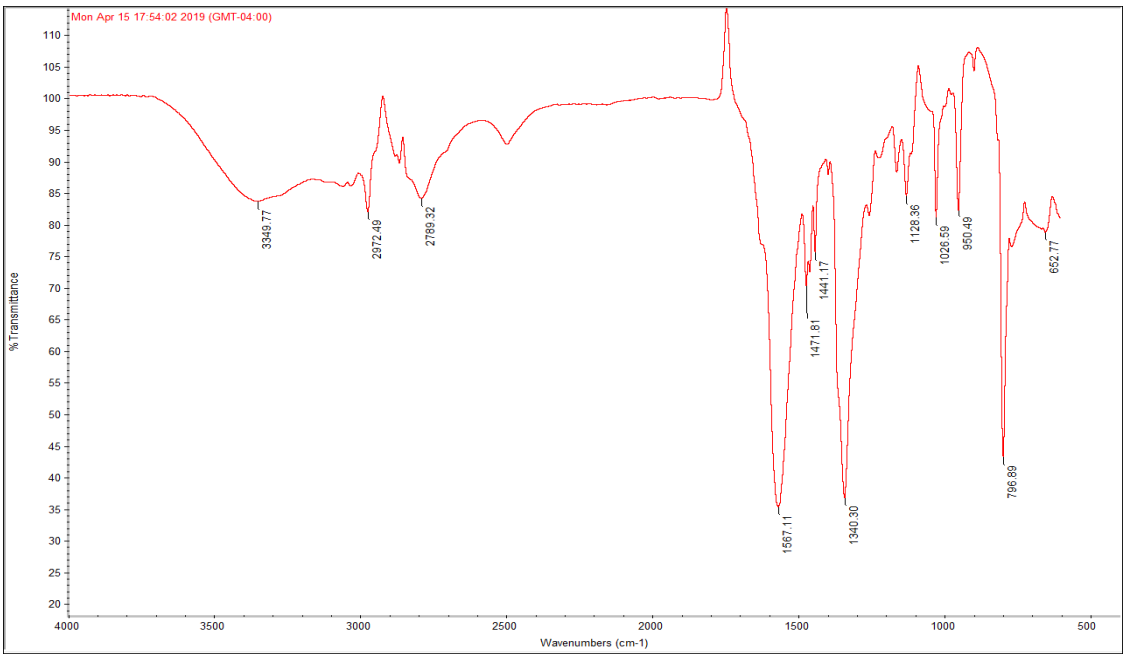

Appendix 9: IR spectra for ZnHIP_ZnCl. Prominent peaks can be observed at 3349.77, 2912.49, 2789.32, 1567.11, 1340.30 cm^{-1}.

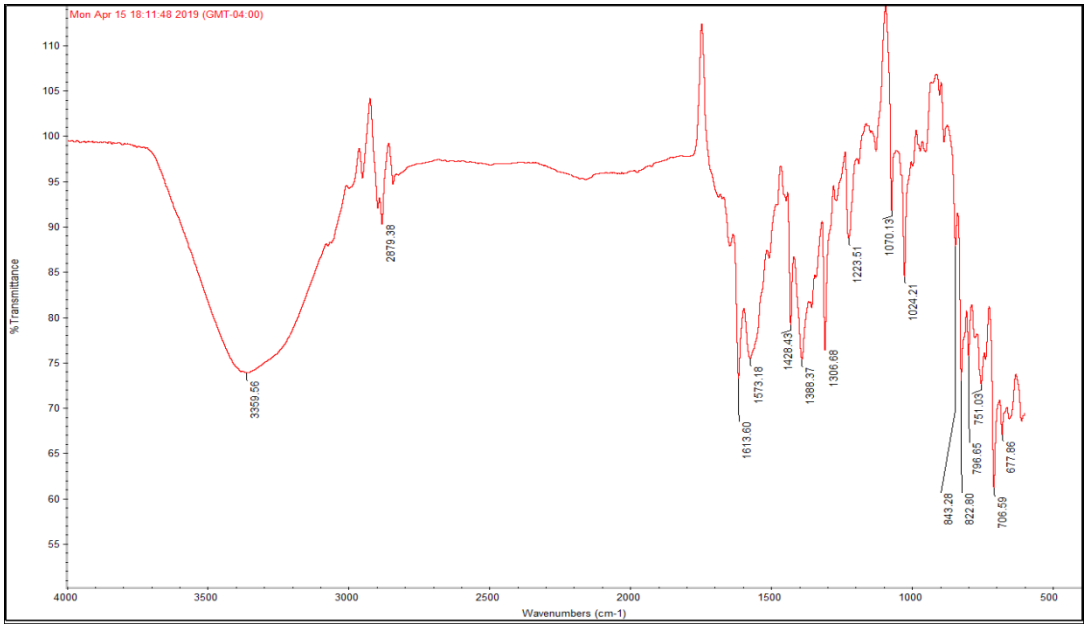

Appendix 10: IR spectra for ZnPheAdamantane. Prominent peaks can be observed at 3359.56, 2879.38, 1613.60, 1573.18, 1306.68 cm^{-1}.

Acknowledgements

I would like to thank the mentorship of Dr. Carmen Gauthier and Dr. Jason Montgomery for their oversight on this project. We also thank Dr. Betty Galarreta, Pontifical Catholic University of Peru, and the grant number: Grant No. 281-INNOVATEPERU-EC-2017 for her assistance with SEM and TEM imaging.

References

1. Cancer Treatment and Survivorship: Facts and Figures 2014-2015. *American Cancer Society*, 2.
2. Coates, A., Abraham, S., Kaye, S. B., Sowerbutts, T., Frewin, C., Fox, R. M., & Tattersall, M. H. N.. *European Journal of Cancer and Clinical Oncology*, *19*(2), **1983** 203-208.
3. Zhao, Y., Trewyn, B. G., Slowing, I. I., & Lin, V. S. Y. *Journal of the American Chemical Society*, **2009**, *131*(24), 8398-8400.
4. Burnier, M., & Biollaz, J. *Clinical pharmacokinetics*, **1992**, *22*(5), 375-384.
5. Kao, H. D., Traboulsi, A., Itoh, S., Dittert, L., & Hussain, A. *Pharmaceutical research*, **2000**, *17*(8), 978-984.
6. Shen, H., & Zhong, M. *Journal of pharmacy and pharmacology*, **2006**, *58*(9), 1183-1191.
7. McNamara, D. P., Childs, S. L., Giordano, J., Iarriccio, A., Cassidy, J., Shet, M. S., & Park, A. *Pharmaceutical research*, **2006**, *23*(8), 1888-1897.
8. Shargel, L., Andrew, B. C., & Wu-Pong, S. *Applied biopharmaceutics & pharmacokinetics* (pp. 32-35). **1999**, Stamford: Appleton & Lange.

9. Uhrich, K. E., Cannizzaro, S. M., Langer, R. S., & Shakesheff, K. M. *Chemical reviews*, **1999**, *99*(11), 3181-3198.
10. Vasconcelos, T., Sarmento, B., & Costa, P. *Drug discovery today*, **2007**, *12*(23-24), 1068-1075.
11. Stuurman, F. E., Nuijen, B., Beijnen, J. H., & Schellens, J. H. *Clinical pharmacokinetics*, **2013**, *52*(6), 399-414.
12. Sharma, D., Chelvi, T. P., Kaur, J., Chakravorty, K., De, T. K., Maitra, A., & Ralhan, R. *Oncology Research Featuring Preclinical and Clinical Cancer Therapeutics*, **1996**, *8*(7-8), 281-286.
13. Chowdhuri, A. R., Singh, T., Ghosh, S. K., & Sahu, S. K. *ACS applied materials & interfaces*, *8*(26), **2016** 16573-16583
14. Sutradhar, K. B., & Amin, M. L. *ISRN Nanotechnology*, **2014**.
15. Sercombe, L., Veerati, T., Moheimani, F., Wu, S. Y., Sood, A. K., & Hua, S. *Frontiers in pharmacology*, **2015**, *6*, 286.
16. Della Rocca, J., Liu, D., & Lin, W. *Accounts of chemical research*, *44*(10), **2011** 957-968.
17. Horcajada, P., Serre, C., Maurin, G., Ramsahye, N. A., Balas, F., Vallet-Regi, M., & Férey, G. *Journal of the American Chemical Society*, **2008**, *130*(21), 6774-6780.
18. Llewellyn, P. L., Horcajada, P., Maurin, G., Devic, T., Rosenbach, N., Bourrelly, S., & Férey, G. *Journal of the American Chemical Society*, **2009**, *131*(36), 13002-13008.
19. Horcajada, P., Chalati, T., Serre. C., Gillete, B., Sebrie, C., Baati, T., Eubank, J., Heurtaux, D., Pascal, C., Kreuz, C., Chang, J., Hwang, Y., Marsaud, V., Bories, P.,

Cynober, L., Gil, S., Ferey, G., Couvrer, P., and Ruxandra Gref. *Nat. Mater.* **2010**, *9*(2), 172.

20. Perry Iv, J. J., Perman, J. A., & Zaworotko, M. J. *Chemical Society Reviews*, **2009**, *38*(5), 1400-1417.
21. Ronson, T. K., Fisher, J., Harding, L. P., & Hardie, M. J. *Angewandte Chemie*, **2007**, *119*(47), 9244-9246.
22. Perry IV, J. J., Kravtsov, V. C., McManus, G. J., & Zaworotko, M. J.. *Journal of the American Chemical Society*, **2007**, *129*(33), 10076-10077.
23. Wang, H. N., Meng, X., Yang, G. S., Wang, X. L., Shao, K. Z., Su, Z. M., & Wang, C. G. *Chemical Communications*, **2011**, *47*(25), 7128-7130.
24. Tian, D., Chen, Q., Li, Y., Zhang, Y. H., Chang, Z., & Bu, X. H. *Angewandte Chemie International Edition*, **2014**, *53*(3), 837-841.
25. Lu, W., Yuan, D., Makal, T. A., Wei, Z., Li, J. R., & Zhou, H. C. *Dalton Transactions*, **2013**, *42*(5), 1708-1714.
26. Caulder, D. L., Powers, R. E., Parac, T. N., & Raymond, K. N. *Angewandte Chemie International Edition*, **1998**, *37*(13-14), 1840-1843.
27. Prakash, M. J., Oh, M., Liu, X., Han, K. N., Seong, G. H., & Lah, M. S. *Chemical Communications*, **2010**, *46*(12), 2049-2051.
28. Brant, J. A., Liu, Y., Sava, D. F., Beauchamp, D., & Eddaoudi, M. *Journal of molecular structure*, **2006**, *796*(1-3), 160-164.
29. Samanta, S. K., Moncelet, D., Vinciguerra, B., Briken, V., & Isaacs, L. *Helv. Chim. Acta*, **2018**, *101*(6).

30. Zhao, D., Tan, S., Yuan, D., Lu, W., Rezenom, Y. H., Jiang, H., & Zhou, H. C. *Advanced Materials*, **2011**, *23*(1), 90-93.

31. Samanta, S. K., Moncelet, D., Briken, V., & Isaacs, L. *J. Am. Chem. Soc.*, **2016**, *138*(43), 14488-14496.

32. Chen, T. H., Wang, L., Trueblood, J. V., Grassian, V. H., & Cohen, S. M. *J. Am. Chem. Soc.*, **2016**, *138*(30), 9646-9654.

33. Horcajada, P., Gref, R., Baati, T., Allan, P. K., Maurin, G., Couvreur, P., ... & Serre, C. *Chemical reviews*, **2011**, *112*(2), 1232-1268.

34. Serre, C., Millange, F., Surblé, S., & Férey, G. *Angewandte Chemie International Edition*, **2004**, *43*(46), 6285-6289.

35. Serre, C., Surblé, S., Mellot-Draznieks, C., Filinchuk, Y., & Férey, G. *Dalton Transactions*, **2008**, (40), 5462-5464.

36. Sun, C. Y., Qin, C., Wang, C. G., Su, Z. M., Wang, S., Wang, X. L., & Wang, E. B. *Advanced Materials*, **2011**, *23*(47), 5629-5632.

37. Zhuang, J., Kuo, C. H., Chou, L. Y., Liu, D. Y., Weerapana, E., & Tsung, C. K. *ACS nano*, **2014**, *8*(3), 2812-2819.

38. Moulton, B., Lu, J., Mondal, A., & Zaworotko, M. J.. *Chemical Communications*, (9), **2001** 863-864.

39. Vetromile, C. M., Lozano, A., Feola, S., & Larsen, R. W. *Inorg. Chem. Acta*, **2011**, *378*(1), 36-41.).

40. Duan, L. N., Dang, Q. Q., Han, C. Y., & Zhang, X. M. *Dalton Transactions*, *44*(4), **2015** 1800-1804.

41. Tian, L., Yang, N., & Zhao, G. Y. *Inorganic Chemistry Communications*, **2010**, *13*(12), 1497-1500.

42. Plater, M. J., Foreman, M. R. S. J., Howie, R. A., Skakle, J. M., McWilliam, S. A., Coronado, E., & Gómez-García, C. J. *Polyhedron*, *20*(18), **2001** 2293-2303.

43. Zhou, D. S., Wang, F. K., Yang, S. Y., Xie, Z. X., & Huang, R. B. *CrystEngComm*, *11*(11), **2009** 2548-2554.

44. Bühl, M., & Kabrede, H. *J. Chem. Theory. Comp.* **2006**, *2*(5), 1282-1290.

45. Bak, J. H., Le, V. D., Kang, J., Wei, S. H., & Kim, Y. H. *The Journal of Physical Chemistry C*, **2012**, *116*(13), 7386-7392.

46. Mueller, T., & Ceder, G. *The Journal of Physical Chemistry B*, **2005**, *109*(38), 17974-17983.

47. Teo, J. M., Coghlan, C. J., Evans, J. D., Tsivion, E., Head-Gordon, M., Sumby, C. J., & Doonan, C. J. *Chemical Communications*, **2016**, *52*(2), 276-279.

48. Torrisi, A., Bell, R. G., & Mellot-Draznieks, C. *Microporous and Mesoporous Materials*, **2013**, *168*, 225-238.

49. van der Wijst, T., Guerra, C. F., Swart, M., & Bickelhaupt, F. M. *Chemical Physics Letters*, **2006**, *426*(4-6), 415-421.

50. Liangliang Zhang, Jie Guo, Qingguo Meng, Rongming Wang, Daofeng Sun, *CrystEngComm*, **2013**, 15, 9578,

51. Zuo-wei Wang, Yi-Zhi Li, Ya Cai, He-Gen Zheng, *Acta Crystallographica Section E: Structure Reports Online*, **2006**, 62.